Combustion and Flame 254 (2023) 112844

Contents lists available at ScienceDirect

Combustion and Flame

journal homepage: www.elsevier.com/locate/combustflame

Computation and prediction of intrinsic thermoacoustic oscillations associated with autoignition fronts

Harish S. Gopalakrishnan[a], Andrea Gruber[b,a], Jonas P. Moeck[a,*]

[a] Department of Energy and Process Engineering, Norwegian University of Science and Technology, Trondheim, 7034, Norway
[b] Thermal Energy Department, SINTEF Energy Research, Trondheim, 7034, Norway

ARTICLE INFO

Article history:
Received 18 November 2022
Revised 8 May 2023
Accepted 8 May 2023

Keywords:
Combustion dynamics
Intrinsic thermoacoustic feedback
Autoignition front
Linear stability
Sequential combustor

ABSTRACT

A sequential combustor architecture consists of two longitudinally staged combustion zones featuring a propagation-stabilized flame in the first stage and an autoignition-stabilized flame in the second (reheat) stage. This layout allows for increased fuel flexibility compared to single-stage systems and enables clean and efficient combustion of carbon-free fuels such as hydrogen. Interactions between the autoignition-stabilized flame and the acoustic field created by the unsteady ignition front and the surrounding boundaries can result in self-sustained (thermoacoustic) flame oscillations in the reheat stage of the sequential burner, causing performance losses and structural damage. In this paper, an intrinsic flame-acoustic feedback mechanism causing self-sustained thermoacoustic oscillations in a reheat combustor is studied. The intrinsic thermoacoustic feedback is established when an acoustic wave generated by the unsteady ignition front travels upstream and introduces local temperature, pressure and velocity perturbations in the unburnt mixture. These modulate the ignition chemistry and the front kinematics and thus, in turn, act as a new source of perturbation for the ignition front that generates heat release rate oscillations and upstream-traveling acoustic disturbances, closing the feedback loop. Compressible reactive Euler equation computations of autoignition fronts in a simple one-dimensional reheat combustor configuration with fully non-reflecting boundaries are first performed to demonstrate and characterize the intrinsic thermoacoustic oscillations associated with autoignition fronts. These computations show that the autoignition front exhibits distinct harmonic thermoacoustic oscillations which tend to become unstable at some conditions. Next, frequencies and growth rates of the intrinsic thermoacoustic oscillations in the linear regime are predicted using a hybrid approach with flame response transfer functions taken from a forced Euler calculation and using a linearized Euler equation framework to describe the combustor acoustic field. The predictions of the intrinsic thermoacoustic eigenvalue from the linearized Euler equation framework show good agreement with the linear behaviour of these oscillations observed in the Euler computations. The findings of the present work are useful both from a fundamental standpoint for prediction of intrinsic thermoacoustic instabilities and from an industrial perspective for prevention of thermoacoustic instabilities in staged combustion systems.

1. Introduction

Increasingly stringent regulations on greenhouse gas emissions from gas turbines used for power generation is motivating a gradual transition to carbon-free fuels such as hydrogen. When highly-reactive hydrogen is burnt in a combustor designed to operate on natural gas, the flame position shifts closer to the combustor inlet resulting in a risk of flashback. An attractive alternative is to separate the combustion process into two stages where, in the first stage, an ultra-lean hydrogen–air mixture is burnt with a propagation-stabilized flame. Thereafter, the rest of the fuel is added to the burnt product mixture exiting from the first stage and, due to the high temperature associated with this vitiated-oxidant mixture, it spontaneously ignites in the second (reheat) stage resulting in the formation of an autoignition front [1]. Thus, varying the fuel splits between the first and second stage in a longitudinally-staged combustion system allows for clean, efficient and fuel-flexible power generation [1,2]. In such a staged combustion system, unsteady interactions between the autoignition front and the acoustic field associated with the unsteady flame and

* Corresponding author.
E-mail address: jonas.moeck@ntnu.no (J.P. Moeck).

https://doi.org/10.1016/j.combustflame.2023.112844

the surrounding boundaries can cause self-sustained oscillations in all flow quantities [3]. This unsteady flow-flame-acoustic coupling phenomena, also known as thermoacoustic/combustion instability, can result in structural damage, loss in performance and can be very detrimental to the efficient operation of the system [4].

Combustion instabilities have been conventionally thought of as a feedback loop involving the combined dynamics of the flame, flow and the resonant acoustic modes of the combustion chamber. Unsteady heat release rate oscillations associated with the flame front generate acoustic waves [5], which travel upstream and downstream and are reflected by the chamber boundaries and in turn perturb the flame, thus closing the feedback loop. In this well-established framework, feedback is not expected to occur if the boundaries of the combustor are perfectly non-reflecting. More recently, the seminal works of Hoeijmakers et al. [6], Emmert et al. [7] and Bomberg et al. [8] proposed an *intrinsic* feedback mechanism through which self-sustained thermoacoustic oscillations may be established even in the absence of acoustic reflection from boundaries (also, see the comprehensive review by Silva [9]), which is discussed next. In these works, propagation-stabilized flames were considered.

Propagating flames are usually stabilized at low values of mean flow Mach numbers, owing to typically low flame speeds associated with reactant mixtures used for gas turbine combustion. The magnitudes of the relative pressure (p'/p_0), temperature (T'/T_0) and velocity (u'/u_0) fluctuations induced by an acoustic wave can be related to each other as [10]

$$\frac{p'}{p_0} = \frac{\gamma}{\gamma - 1}\frac{T'}{T_0} = \gamma M_0 \frac{u'}{u_0}, \tag{1}$$

where M_0 is the mean flow Mach number, and γ is the ratio of specific heats. At low Mach numbers typical of propagation-stabilized flames, the normalized pressure and temperature oscillations are, hence, much smaller than the normalized velocity oscillations. Thus, the propagation-stabilized flame does not directly respond to acoustic waves, but primarily to velocity oscillations induced by the acoustic wave upstream of the flame front. These velocity oscillations can induce a flame response, for example, by creating equivalence ratio fluctuations at the fuel injector [11] or by creating a vortical wave at the swirler upstream of the flame [12]. The unsteady heat release rate oscillations ($\dot{Q}'$) created by the velocity oscillations generate upstream-traveling acoustic waves, which in turn cause perturbations upstream of the flame front and closes the feedback loop. Thus, feedback between the flame dynamics and the velocity perturbations induced by the upstream-traveling acoustic disturbances can result in intrinsic thermoacoustic (ITA) instability even in the absence of acoustic wave reflection from the boundaries. Intrinsic thermoacoustic modes associated with propagation-stabilized flames have been observed both in experiments [6,8], flow computations [13,14] and analytical models [7,15,16].

Intrinsic thermoacoustic feedback is expected to be highly relevant for autoignition fronts, too, because of the following reasons. Autoignition fronts reside at locations in the combustor where the ignition time of the reactant mixture is equal to the residence time. Unlike the case of a propagating flame where the advection–diffusion–reaction balance governs the flame position to leading order, the balance between the advective and the chemical time scales governs the location of an autoignition front. Typical ignition times of vitiated hydrogen–air mixtures at reheat conditions are usually very small, i.e., of the order of a few milliseconds or less. At these conditions, mean flow velocities of the order of a few hundred m/s are required to maintain the ignition front at desirable locations inside the combustor, which correspond to non-negligible values of Mach numbers ($0.25 - 0.3$). At such finite values of Mach numbers, the normalized pressure and temperature fluctuations have comparable magnitudes to the normalized velocity oscillations [Eq. (1)]. The pressure and temperature oscillations induced by the upstream-traveling acoustic waves modulate the chemical kinetic processes associated with spontaneous ignition, which modulates the ignition time of the reactant mixture, and therefore the ignition front position, over one cycle of acoustic forcing. The fluctuations in the ignition front position create significant oscillations in the global and local heat release rate [17,18], which in turn induces upstream-traveling acoustic disturbances [19], thereby closing the feedback loop. This mechanism of combustion instability was first investigated in the context of sequential combustors by Ni et al. [20] who proposed and validated, with engine measurements, a simple numerical model to predict the frequencies and growth rates of thermoacoustic oscillations in an idealized combustor configuration.

Figure 1(a) plots the variation of the ignition time (τ) of a reactant mixture with temperature (T). A constant-pressure reactor calculation in Cantera [21] with static variations in temperature is used to generate Fig. 1(a). As expected, an increase in temperature accelerates the ignition chemistry and results in a decrease in ignition time. A parameter (ψ) can now be defined to quantify the sensitivity of the ignition time to small changes in temperature as

$$\psi(T_0) = \frac{(\partial\tau/\partial T)_{T_0}}{\tau_0/T_0}, \tag{2}$$

where a small change in temperature δT centered around a temperature T_0 results in a small change in ignition time $\delta\tau$ centered around an ignition time τ_0. The quantity ψ, which is plotted in Fig. 1(b), measures the relative change in ignition time induced by a change in temperature. In the band of temperatures between 950 to 1000 K, small changes in reactant temperatures (created by an acoustic wave, say) result in much larger changes in the mixture ignition time, which leads to significant oscillations in the ignition front position and heat release rate, potentially driving intrinsic thermoacoustic oscillations. Therefore, intrinsic thermoacoustic feedback can be quite important for autoignition fronts, given that small changes in temperature and pressure can significantly change the ignition front position and heat release rate by perturbing the ignition chemistry.

For combustors containing propagating flames, Mukherjee and Shrira [15] showed that ITA modes are infinitely damped in the limit of low flame response gain and become less stable as the gain is increased. Additionally, Hoeijmakers et al. [6] and Emmert et al. [7] derived a simple criterion to show that for a one-dimensional propagating flame, unstable ITA modes can result when the flame response gain is higher than a certain critical value (see Eq. (11)). While a simple criterion for ITA instability does not currently exist for autoignition fronts, it can be deduced by extrapolation that the high sensitivity of the ignition time to temperature fluctuations can result in significant flame response gains for autoignition fronts, thus, favouring intrinsic thermoacoustic instability. The inset in Fig. 1(b) plots the frequency and growth rate of the ITA oscillations obtained from reactive Euler equation computations of autoignition fronts at different inlet temperatures. The autoignition front tends to be progressively less stable (growth rate increases), in an intrinsic thermoacoustic sense, as the inlet temperature approaches the maximum of the ψ vs T curve.

To study intrinsic thermoacoustic oscillations associated with an autoignition front, we consider a simplified one-dimensional (1D) combustor (Fig. 2) with a perfectly premixed reactant mixture entering the inlet at a sufficiently high temperature, resulting in autoignition at a downstream location X_{ig0}. The boundaries are fully non-reflecting, and acoustic (f_1, g_2) and entropy (h_1) forcing are applied at the inlet (f_1, h_1) and the exit (g_2) to study flame dynamics.

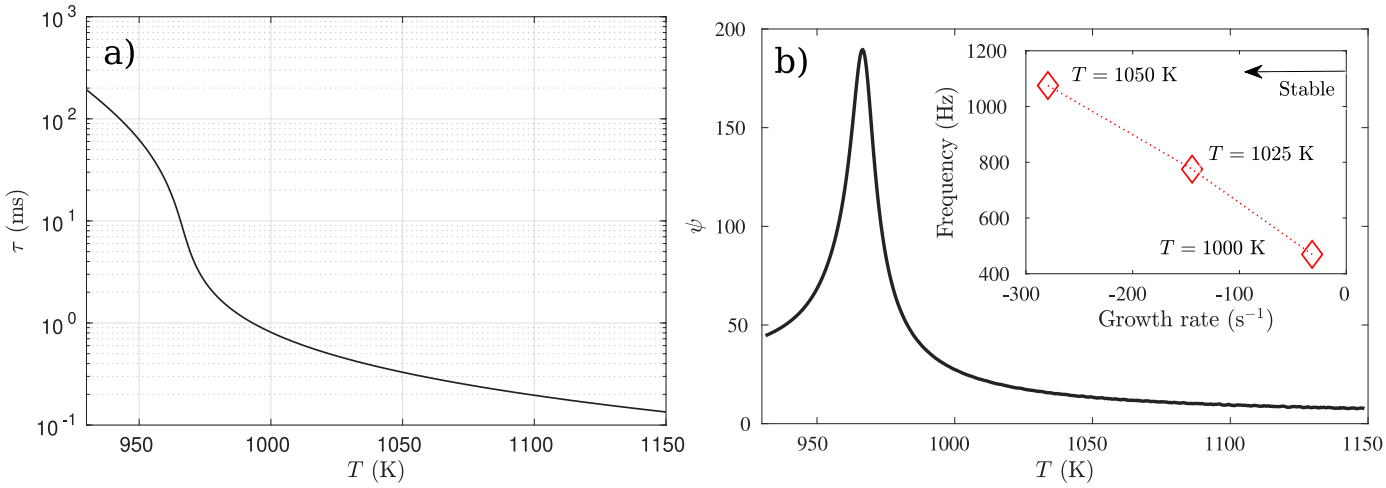

Fig. 1. (a) Variation of the ignition time of a vitiated hydrogen–air mixture with temperature. The equivalence ratio of the reactant mixture is 0.12, and the pressure is 1 atm. (b) Sensitivity of the ignition time to small changes in temperature. The inset in (b) shows the frequency and growth rate of the ITA oscillations associated with the autoignition front at different inlet temperatures.

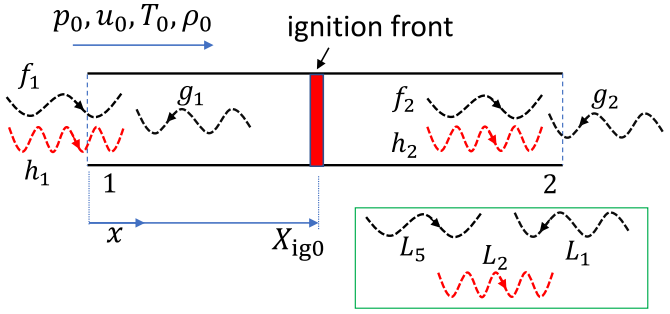

Fig. 2. Schematic of the one-dimensional configuration used throughout this article. The various waves propagating in the domain are shown. The green box shows the waves nomenclature adopted in the NSCBC formulation. Waves coloured in black are acoustic, while the ones coloured in red are entropic. (For interpretation of the references to colour in this figure legend, the reader is referred to the web version of this article.)

The acoustic–flow–flame interactions causing the ITA feedback in autoignition fronts is schematically depicted in Fig. 3, which represents the signal flow graph of an active flame placed in an anechoic environment (as in Fig. 2). This graph is inspired by similar ones constructed for propagation-stabilized flames by Emmert et al. [7] and Bomberg et al. [8]. It is to be noted that the entropy wave imposed at the inlet is assumed to be zero. This does not change the dynamics of the ITA feedback, and is done purely to make the signal flow graph more presentable. Each of the blocks in Fig. 3 represent a frequency dependent transfer function relating the output to the input. The outgoing waves are generated, partly, by the transmission and reflection of the imposed acoustic and entropy waves due to the change in acoustic impedance associated with the ignition front (blocks T_i and R_i - also see Eq. (13) for the definition of these blocks). For example, the g_1 wave is created by the reflection of the wave f_1 via the transfer function R_1 and transmission of the wave g_2 via the transfer function T_1. In addition to this mechanism, the waves f_1 and g_1 introduce temperature, pressure and velocity perturbations in the unburnt reactant mixture, modulating the ignition chemistry and the front kinematics thereby creating harmonic heat release rate ($\dot{Q}'$) and flame position (X'_{ig}) fluctuations via the flame response functions $\mathcal{F}$ and $\mathcal{G}$. Finally, these heat release rate and position fluctuations associated with an autoignition front also generate outgoing acoustic and entropy waves f_2, g_1 and h_2 via the transfer function $\mathcal{S}_{f2}, \mathcal{S}_{g1}$ and $\mathcal{S}_{h2}$. Thus, we have the intrinsic thermoacoustic feedback loop shown in dashed lines in Fig. 3, consisting of the g_1 wave modifying the flow and creating a flame response via $\mathcal{G}$ and the unsteady flame generating a g_1 wave via $\mathcal{S}_{g1}$.

Gruber et al. [22] and Gopalakrishnan et al. [23] performed Navier–Stokes and Euler computations of the initial ignition process of hydrogen autoignition fronts in a one-dimensional configuration similar to Fig. 2. They observed that the ignition front exhibits significant harmonic oscillations in its position and heat release rate before attaining steady state (see Fig. 8). This, they hypothesized, was due to an intrinsic interaction mechanism between the flame dynamics and the upstream-traveling acoustic disturbances. While these works provide initial evidence of the occurrence of ITA oscillations in autoignition fronts, a detailed characterization of these oscillations using flow computations is essential.

Detailed flow computations give useful insight into the intrinsic thermoacoustic oscillations in reheat combustion systems. From an industrial standpoint, however, an efficient framework capable of predicting the linear stability of the ITA oscillations in simple reheat combustor configurations would be very useful. A linear stability analysis for thermoacoustic systems requires two essential elements. The first one is a model for the flame response, in terms of the unsteady heat release rate, to acoustic and convective perturbations. The vital component of such a model is the frequency-dependent flame transfer function (FTF), which relates the global heat release rate to the acoustic perturbations [24,25]. The second required element is a model for the combustor acoustic field. This is simply a set of (possibly simplified) equations which govern the generation and propagation of acoustic and entropic perturbations in a flow domain. For an inviscid 1D flow at non-zero Mach numbers, the linearized Euler equations model the generation and propagation of small disturbances [26]. When applied to reacting flows in the limit of zero Mach number where entropy wave propagation is neglected, these equations reduce to a single wave equation in terms of the acoustic pressure perturbations, or the Helmholtz equation in frequency domain [10,27]. As an additional simplification, the acoustic field of many combustor configurations have been modeled by a low-order network approach consisting of a collection of interconnected elements which model area

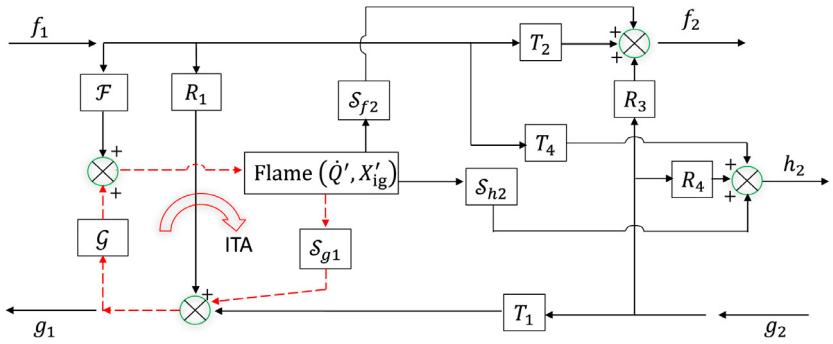

Fig. 3. Signal flow graph of an active flame in an acoustic environment without reflection from the boundaries. Each block represents a frequency-dependent transfer function relating the output to the input. The intrinsic thermoacoustic feedback loop is represented by the dashed lines composed of: the upstream-traveling (g_1) wave modifying the flow, the flame response to the g_1 wave – $\mathcal{G}$, and the unsteady flame response generating a g_1 wave – $\mathcal{S}_{g1}$.

changes, boundary conditions and active flame elements [14,28–30]. A transfer matrix relating the pressure and velocity perturbations upstream and downstream of each sub-element is formulated, and the full system matrix is obtained from assembling all sub-elements. Thus, the flame response model in conjunction with the model for the acoustic field of the combustor yields the thermoacoustic eigenvalue(s) of the full system, giving quantitative insight into the frequencies and growth rates of the thermoacoustic modes.

In the context of thermoacoustic modeling of reheat combustors, Zellhuber et al. [31], Gant et al. [17] and Gopalakrishnan et al. [18] have proposed simplified models for computing the response of an autoignition-stabilized flame to acoustic and entropy perturbations. All these works treat the flow as a collection of independently evolving fluid particles and the global flame response is constructed by stitching together the individual particle evolution. An important aspect to consider when modeling the response of an autoignition front to acoustic perturbations is the continuous modulation of the chemical state of the reactant mixture by the acoustic wave during its downstream advection [18]. Simple models based on the balance of flow residence time and mixture ignition time are insufficient for acoustically perturbed autoignition fronts, and the continuous modulation of the ignition chemistry by the acoustic temperature and pressure fluctuations needs to be accounted for. Gant et al. [32] and Gopalakrishnan et al. [23] proposed simplified frameworks based on the Rankine–Hugoniot jump conditions and the linearized Euler equations, respectively, to model the acoustic field associated with an unsteady autoignition front. While simplified models for the flame response and the acoustic field have been proposed, an effort to use them and predict the linear stability of intrinsic thermoacoustic oscillations associated with an autoignition front and compare these predictions with more detailed approaches has not yet been performed. This the main focus of this article.

The primary objectives of the present work are the following:

1. To perform unsteady reactive Euler equation computations to establish the occurrence and characterize the linear dynamics of the intrinsic thermoacoustic oscillations associated with autoignition fronts in a one-dimensional setting as depicted in Fig. 2. This is discussed in Section 2.
2. To predict the linear stability of the ITA oscillations using a hybrid approach where the flame response functions, extracted from forced Euler equation computations, are used within a linearized Euler equation framework [23]. The predictions from this hybrid approach are compared to the linear thermoacoustic eigenvalue obtained from the flow computations performed to meet Objective 1. These results are presented in Section 3.

In the present work, all flow computations are performed within an Euler equation framework. This is mainly motivated by the prior results of Gopalakrishnan et al. [23], who compared Euler and Navier–Stokes [22] computations of intrinsic thermoacoustic oscillations observed during the initial ignition process of an autoignitive mixture. These comparisons revealed identical ignition front behaviour and identical frequencies and growth rates of the ITA oscillations, suggesting that diffusive effects (viscosity, heat conduction and species diffusion) play a relatively minor role in the dynamics of the ITA feedback associated with the autoignition front, at least in the present one-dimensional setting. However, diffusive effects contribute to the dispersion and dissipation of entropy waves which are convected from the first-stage of the sequential burner downstream to the autoignition front [17,33,34], and therefore must be taken into account in realistic combustor systems.

2. Intrinsic thermoacoustic oscillations from forced Euler computations of autoignition fronts

In this section, the occurrence of intrinsic thermoacoustic oscillations associated with autoignition fronts is demonstrated by way of reactive Euler equation computations. Section 2.1 presents the framework used to perform these computations and Section 2.2 discusses the results. The geometrical configuration that is considered is a simplified 1D combustor model introduced in Section 1 and schematically depicted in Fig. 2.

2.1. Computational framework

The equations governing the flow of an inviscid reactive fluid in one spatial dimension (x) can be written in compact form as [35]

$$\frac{\partial \mathbf{U}}{\partial t} + \mathbf{A}\frac{\partial \mathbf{U}}{\partial x} = \mathbf{S}, \tag{3}$$

where $\mathbf{U}$ is the vector containing the primitive variables density, velocity, pressure and species mass fractions: $[\rho, u, p, Y_i]^{\mathrm{T}}$, the second term represents all the terms involving the spatial derivatives, and $\mathbf{S}$ is the vector of the source terms: $[0, 0, S_p, S_{Y_i}]^{\mathrm{T}}$. The matrix $\mathbf{A}$ in the non-linear convective term is a function of $\mathbf{U}$. In writing the above equations, body forces were neglected.

Non-reflecting boundary conditions (NRBC's) are imposed for the flow computations since we wish to study intrinsic thermoacoustic oscillations. The basic principle behind the formulation of the NRBC's is that the waves traveling from the interior of the computational domain towards the boundaries should leave the domain unaltered and unreflected. Furthermore, we model a fully premixed reactant mixture entering the inlet of the computational domain at all time instants, which implies fixed values of species

Table 1
Values of the characteristic variables, wave amplitudes and source terms in Eq. (4). The wave indices correspond to the classical NSCBC nomenclature [36,37], where indices 3 and 4 represent the advection of transverse velocity components which are absent in the present one-dimensional configuration. S_p and S_{Y_i} denote the source terms of the energy and the ith species mass balance equations, respectively [35,38].

Index (j)	$d\mathcal{W}_j$	$\mathcal{L}_j$	$\mathcal{S}_j$
1	$dp - \rho c du$	$(u-c)\left(\frac{\partial p}{\partial x} - \rho c \frac{\partial u}{\partial x}\right)$	S_p
2	$c^2 d\rho - dp$	$u\left(c^2 \frac{\partial \rho}{\partial x} - \frac{\partial p}{\partial x}\right)$	$-S_p$
5	$dp + \rho c du$	$(u+c)\left(\frac{\partial p}{\partial x} + \rho c \frac{\partial u}{\partial x}\right)$	S_p
Y_i	dY_i	$u \frac{\partial Y_i}{\partial x}$	S_{Y_i}

mass fractions at the inlet. In practice, upstream-traveling acoustic disturbances cause velocity oscillations at the fuel injector location [11] resulting in equivalence ratio fluctuations convecting downstream. For example, a positive velocity oscillation at a 'stiff' fuel injector results in a leaner mixture and vice-versa. While this mechanism of creation of equivalence ratio fluctuations by the upstream-traveling acoustic wave also contributes to the ITA feedback, this is not taken into account in this work. We only focus on the modulation of the ignition chemistry and the front kinematics by the upstream-traveling acoustic waves as the primary mechanism for ITA feedback.

NRBC's are imposed by making use of the Navier–Stokes characteristic boundary condition (NSCBC) formulation [36,37]. The Euler Eq. (3) at the boundary points are first transformed in terms of the characteristic variables by applying a similarity transformation to the matrix **A**. After this transformation, Eq. (3) reduces to a set of 1D advection equations at the boundary points:

$$\frac{\partial \mathcal{W}_j}{\partial t} + \mathcal{L}_j = \mathcal{S}_j, \tag{4}$$

where $\mathcal{W}_j$ represents the characteristic variables, which are simply the acoustic and convective waves traveling with the speeds $u-c, u+c$ and u, where c is the local speed of sound, and u is the local flow velocity at the boundary point. The spatial derivatives are contained within $\mathcal{L}_j$, which denotes the characteristic wave amplitudes, and $\mathcal{S}_j$ are the source terms at the characteristic level. Thus, the NSCBC approach transforms the governing equations at the boundary points in terms of advection equations governing the propagation of characteristic waves at the boundaries.

The characteristic wave amplitudes $\mathcal{L}_j$'s are composed of the upstream-traveling acoustic wave ($\mathcal{L}_1$), the downstream-traveling acoustic wave ($\mathcal{L}_5$), the downstream traveling entropy wave ($\mathcal{L}_2$), and the downstream traveling convected wave ($\mathcal{L}_{Y_i}$), which conveys information about the ith species mass fraction. The direction of propagation of the acoustic and entropy waves are depicted in Fig. 2 for a subsonic flow in the positive x-direction. At any boundary point (for example, the inlet), some waves ($\mathcal{L}_5, \mathcal{L}_2, \mathcal{L}_{Y_i}$) enter the computational domain from the exterior, while the others ($\mathcal{L}_1$) leave the computational domain. The expressions for the characteristic variables, wave amplitudes and source terms in Eq. (4) are given in Table 1.

Thus, the implementation of the boundary conditions amounts to solving Eq. (4) where, the amplitudes of the waves ($\mathcal{L}_j$'s) entering the domain need to be specified, while the amplitudes of the waves leaving the domain are computed using the interior data. Fully non-reflecting boundary conditions are realized when the time rate of change of the characteristic variables entering the computational domain are zero [37], that is,

$$\frac{\partial \mathcal{W}_j}{\partial t} = 0 \Rightarrow \mathcal{L}_j = \mathcal{S}_j, \tag{5}$$

for any wave $\mathcal{L}_j$ entering the computational domain.

The wave amplitudes imposed at the boundaries is written next, following [39,40]. At the inlet boundary

$$\mathcal{L}_5 = S_p + \left\{-2\rho c \frac{\partial u_t}{\partial t} + K\rho c(u - u_{01t} - u_t - u_-)\right\},$$
$$\mathcal{L}_2 = -S_p + \left\{-c^2 \frac{\partial \rho_t}{\partial t} + Kc^2(\rho - \rho_{01t} - \rho_t - \rho_- - \rho_{\mathcal{L}_5})\right\},$$
$$\mathcal{L}_{Y_i} = S_{Y_i}, \tag{6}$$

and at the outlet boundary

$$\mathcal{L}_1 = S_p + \left\{-2\frac{\partial p_t}{\partial t} + K(p - p_{02t} - p_t - p_+)\right\}, \tag{7}$$

where the terms within the curly braces are used to impose the acoustic/entropy forcing. In Eqs. (6) and (7), p_t, u_t and ρ_t represent the target values of pressure, velocity and density oscillations induced by the imposed disturbances $\mathcal{L}_1, \mathcal{L}_5$ and $\mathcal{L}_2$, respectively, and p_{02t}, u_{01t} and ρ_{01t} are the target mean values of the exit pressure, inlet velocity and inlet density, respectively. K is a parameter representative of an inverse time constant given by $\sigma c(1-M^2)/l$, where l is the axial length of the combustor equal to 0.3 m, M is the local Mach number, and the constant σ is set to 0.5. The magnitude of σ depends on how fast any deviation of the inlet value from the target is to be corrected [40]. It is important to note that p_t, u_t and ρ_t only represent the fluctuating quantities associated with the incoming waves and not the fluctuating values of the primitive variables themselves at the boundary points. The pressure fluctuations at the exit boundary, for example, will be the sum of p_t and the pressure fluctuation (p_+) induced by the downstream traveling acoustic wave $\mathcal{L}_5$.

In Eqs. (6) and (7), the flow perturbations induced by the acoustic waves traveling from the interior of the computational domain towards the boundaries are determined from a simple time integration of the corresponding characteristic wave amplitudes [40], for example,

$$p_+ = -\frac{1}{2}\int_0^t \mathcal{L}_5(l,t)dt. \tag{8}$$

The Euler Eq. (3) at the interior points, together with the boundary conditions [Eqs. (4), (6) and (7)] are solved numerically using a fourth-order accurate finite-difference scheme for spatial discretization and a second-order accurate multi-level time stepping scheme for time marching [41]. The combustor domain is discretized on a uniform grid of 15 000 points corresponding to a spatial resolution of 20 μm, which was found to be sufficient to resolve all the chemical and convective length scales associated with this flow. A constant time step of 4 ns was used to march the equations in time. In addition, a detailed chemical mechanism for hydrogen–air combustion, consisting of 9 species and 21 reactions [42] is used for computing the source terms in the energy and the species mass balance equations. The adequacy of the numerical scheme, the grid and time step size in computing this flow was already established in [23] by way of comparison of the unforced Euler computations with a well established DNS solver [43]. Nevertheless, results comparing the forced Euler computations with corresponding Navier–Stokes results obtained from a well-established DNS solver are given in the supplementary material.

2.2. Results: Characterization of ITA oscillations by forced Euler computations

The characterization of the linear intrinsic thermoacoustic modes of the autoignition front can be obtained by computing the

Table 2
Parameters characterizing the mean autoignition front solution, which is taken as the initial condition and then perturbed for the Gaussian-Evolution and forced response computations.

Mean flow parameters			
p_{02t} (Pa)	u_{01t} (m/s)	ρ_{01t} (kg/m^3)	M_0
101,325	200	0.3016	0.29
Species mass fractions			
Y_{H_2}	Y_{O_2}	Y_{H_2O}	Y_{N_2}
0.0081	0.1832	0.0518	0.7569

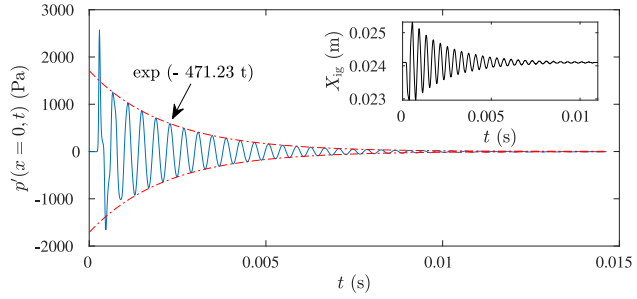

Fig. 4. Evolution of the inlet pressure fluctuations and the ignition front position (inset) for the Gaussian-Evolution computation.

impulse response of the system, i.e., the response of the flow and the flame to an impulse applied at $t = 0$. Of course, in a flow computation, an ideal impulse forcing cannot be imposed (since the magnitude of an ideal impulse tends to infinity, and the thickness tends to zero). The Gaussian function with a unit area and a small thickness is, nevertheless, a good approximation. We first present results wherein an autoignition front stabilized in the one-dimensional combustor with perfectly non-reflecting boundaries is perturbed by a Gaussian pressure pulse (referred to hereafter as Gaussian-Evolution computation). Unforced computations of the initial ignition process of an unburnt reactant mixture are first performed to obtain a stabilized autoignition front [23]. This provides the initial state (Table 2), which is thereafter perturbed by an impulse. A Gaussian pressure pulse which takes the form

$$\frac{1}{\eta\sqrt{2\pi}}\exp\left(-\frac{(x-x_g)^2}{2\eta^2}\right) \tag{9}$$

is superimposed to the initial state at $t = 0$ and evolved in time. In addition, no forcing is imposed at the boundaries. In Eq. (9), η is the thickness of the Gaussian pulse, and x_g is the axial location of the pulse, which is taken to be at the center of the computational domain ($x_g/l = 0.5$) whereas the ignition front is located further upstream at $x/l = 0.08$.

Figure 4 illustrates the response of the autoignition front to the Gaussian pressure pulse in terms of the inlet pressure and flame position. With fully non-reflective boundary conditions, it is somewhat counter-intuitive to observe an oscillatory response of the inlet pressure. One would rather expect that the pulse reaches the boundaries and simply gets flushed out of the domain. However, the harmonic response of the ignition front is no longer surprising if we take into account intrinsic thermoacoustic feedback. The Gaussian pulse travels upstream and creates a flow perturbation in the reactant mixture causing perturbations in heat release rate and flame position, which in turn generates an upstream-propagating acoustic wave and thus, the ITA mode of the system is excited. The oscillations depicted in Fig. 4 occur in all flow variables and exhibit a distinct frequency of 2500 Hz with a temporal growth rate of -75 s^{-1}.

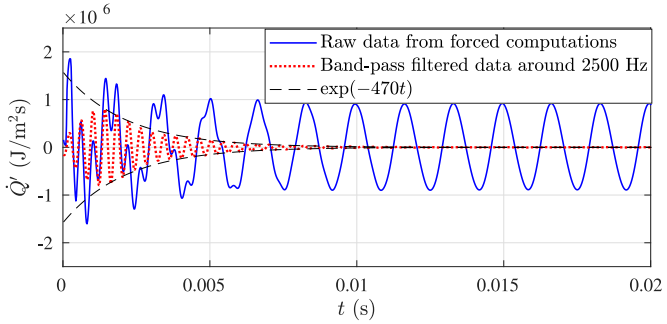

Fig. 5. Integrated heat release rate oscillations of the autoignition front when forced by an entropy wave at the inlet at a frequency of 600 Hz. The intrinsic thermoacoustic oscillations are visible as the high frequency component superimposed on top of the response at the forcing frequency at the initial few time instants ($t < 0.005$ s).

We characterize the ITA oscillations from harmonically forced flow computations next. The steady autoignition front, with mean flow parameters listed in Table 2, is forced by acoustic and entropy waves at the boundaries. Three linearly independent forcing configurations are realized using the forced NSCBC formulation (Section 2.1): (i) acoustic forcing at the inlet with the wave $\mathcal{L}_5$, (ii) entropy forcing at the inlet with the wave $\mathcal{L}_2$, and (iii) acoustic forcing at the exit with the wave $\mathcal{L}_1$. The amplitude of the imposed disturbances are maintained to be small ($0.1 - 0.5\%$ of the mean values) to ensure linear flame dynamics.

Figure 5 shows the response of the autoignition front, in terms of the integrated heat release rate fluctuations, when forced by an entropy wave at the inlet with a frequency of 600 Hz. An interesting aspect to note in the flame response is the high frequency component superimposed on the response at the forcing frequency at the initial few time instants. A Fourier decomposition of the data reveals that this high-frequency oscillation occurs at 2500 Hz, which is the frequency of the ITA mode obtained from the Gaussian-Evolution computation. In addition, the growth rate associated with these superimposed high-frequency oscillations can be computed by band-pass filtering the heat release rate response in Fig. 5 close to 2500 Hz, and using a Hilbert transform to determine the signal envelope [44]. This process yields a growth rate of -74.5 s^{-1}, which agrees well with the value obtained for the growth rate of the ITA mode from the Gaussian-Evolution computation. Analogy can be drawn between the behaviour of the ignition front in Fig. 5 to the forced vibration of a spring-mass-damper system having a specific natural frequency and damping rate. The initial condition associated with the system excites oscillations at the system's natural frequency (in the case of an autoignition front, the frequency of the ITA mode), which, for a viscous damper with positive damping (damped ITA mode), manifests as harmonically decaying oscillations superimposed on the response at the forcing frequency [45].

The heat release rate response of the autoignition front to acoustic forcing at the inlet via an $\mathcal{L}_5$ wave at three distinct frequencies is plotted in Fig. 6. The velocity fluctuations imposed by the $\mathcal{L}_5$ wave take the form $-u_t \sin(\omega t)$, where ω is the angular frequency of the forcing and u_t is maintained at 0.5% of the mean velocity for all frequencies. Although the amplitudes of the imposed disturbances are the same across the different frequencies, large flame response amplitudes are observed when the forcing frequency is equal to the frequency of the ITA mode, signifying an internal resonance occurring in the system due to the ITA feedback.

Further evidence, and characterization, of the ITA oscillations associated with the autoignition front can be obtained by comput-

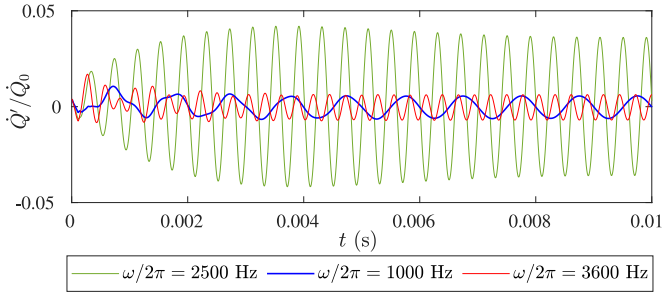

Fig. 6. Integrated heat release rate fluctuations associated with the autoignition front when forced by acoustic waves at the inlet with a constant amplitude of $u'/u_0 = 0.5\%$. The flame response exhibits large amplitudes at 2500 Hz.

ing its scattering matrix. The scattering matrix is a useful concept that has been extensively used in the past for studying intrinsic thermoacoustic oscillations in combustors with propagation-stabilized flames [6–8]. The scattering matrix relates the outgoing characteristic waves to the incoming characteristic waves in frequency domain and thus, unlike the transfer matrix, offers an inherently causal representation of the flame–acoustic coupling. Furthermore, the eigenvalues of the ITA modes of the system can be obtained from the poles of the scattering matrix [6,8]. For the present one-dimensional flow configuration depicted in Fig. 2, the scattering matrix can be written as

$$\begin{bmatrix} f_2 \\ g_1 \\ h_2 \end{bmatrix} = \begin{bmatrix} S_{11} & S_{12} & S_{13} \\ S_{21} & S_{22} & S_{23} \\ S_{31} & S_{32} & S_{33} \end{bmatrix} \begin{bmatrix} f_1 \\ g_2 \\ h_1 \end{bmatrix}, \tag{10}$$

where the expressions for the various characteristic waves are derived by performing a characteristic variable transformation of the linearized Euler equations [46]. The expressions for the characteristic waves are

$$\begin{aligned} g &= (\widetilde{p} - \rho_0 c_0 \widetilde{u})/2, \\ f &= (\widetilde{p} + \rho_0 c_0 \widetilde{u})/2, \\ h &= c_0^2 \widetilde{\rho} - \widetilde{p}. \end{aligned} \tag{11}$$

The quantities with the tilde in Eq. (11) denote the Fourier-decomposed complex-valued quantities representing the amplitude and phase of the corresponding fluctuations in time domain. The waves f_1, g_1 and h_1 are measured at the inlet boundary ($x = 0$), while the waves f_2, g_2 and h_2 are measured at the exit boundary ($x = l$). At a given frequency, all the elements of the scattering matrix can be obtained from the three independent forced Euler calculations.

Figure 7 plots the gain and phase of two representative elements of the scattering matrix obtained from the forced Euler computations of the autoignition front. A distinct peak in the gain is visible at a frequency of 2500 Hz implying significant amplification of the incoming waves, which also points towards a resonance with the ITA mode in the system at that frequency. The other elements of the scattering matrix exhibit qualitatively similar behaviour, and are shown in the supplementary material. For frequency-domain variables we stipulate $z(t) \sim e^{i\omega t}$. The real part of ω is, hence, the angular frequency and the negative imaginary part the growth rate. The associated Laplace variable is $s = i\omega$, so that the real part of s corresponds to the growth rate, and the imaginary part to the angular frequency. System identification tools commonly work with s instead of ω; therefore, in this article, we interchangeably use both notations.

Figure 8 plots the poles of each element of the scattering matrix. The poles of each frequency-dependent term (S_{ij}) were determined using a system identification tool (Vectorfit [47]). The complex variable $s = i(\omega_r + i\omega_i)$ is plotted. Therefore, the real axis represents the growth rate and the imaginary axis represents the frequency of the relevant mode of the system. The dashed blue and red lines denote the frequency and growth rate of the ITA mode obtained from the Gaussian-Evolution computation. While each element of the scattering matrix has a set of poles all distributed in the stable left half-plane, a set of common poles of all the elements of S_{ij} are clustered very close to the imaginary axis around -75 ± 2500i. These least stable poles are listed in Table 3 and indeed show that all the elements of the scattering matrix have a common denominator, whose zeros lie close to -75 ± 2500i. This observation prompts us to factor out the common denominator $D(s)$ from all the elements of the scattering matrix, analogous to what was done for propagation-stabilized flames in [7,8], and the dynamics of the ITA feedback is governed by the zeros of this frequency dependent function. At frequencies where $D(s) = 0$, small-amplitude forcing applied to the system results in significantly amplified system responses.

We conclude this section by highlighting that intrinsic thermoacoustic oscillations are generally present in reheat combustion systems with autoignition fronts. The ITA feedback, for an intrinsically stable system, manifests as damped harmonic oscillations in the forced flame computations. Furthermore, the linear dynamics of the ITA feedback, in terms of the frequency and the growth rate, were obtained from the flow computations using various approaches showing excellent overall agreement.

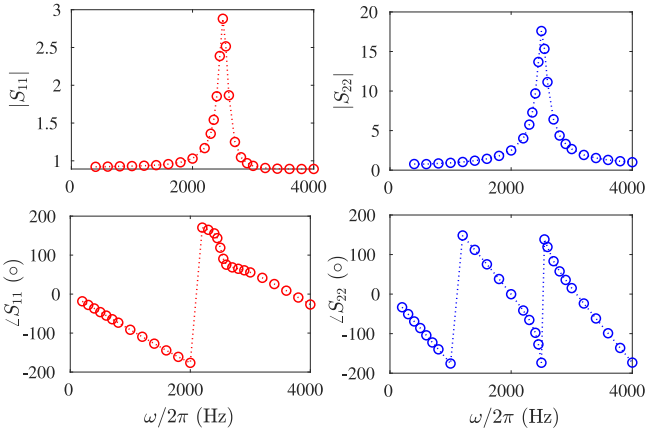

Fig. 7. Representative elements of the scattering matrix of the autoignition front. A distinct peak in gain is visible at 2500 Hz signifying a resonance originating from the ITA mode.

Table 3
Least stable pole $s/2\pi$, where $s = i\omega$, of each element of the scattering matrix associated with the autoignition front.

S_{11}	S_{12}	S_{13}
-74.1 ± 2508.1i	-72.7 ± 2507.5i	-72.1 ± 2508.2i
S_{21}	S_{22}	S_{23}
-73.1 ± 2509.7i	-72.9 ± 2508.1i	-73.2 ± 2508.2i
S_{31}	S_{32}	S_{33}
-73.5 ± 2507.3i	-72.7 ± 2506.1i	-70.2 ± 2508.2i

3. Prediction of ITA oscillations associated with the autoignition front

In this section, we propose a methodology for predicting the linear dynamics of an ITA mode associated with the autoignition front in the one-dimensional configuration (Fig. 2). This is achieved with a frequency-dependent flame response model extracted from the forced Euler computations, in combination with a linearized

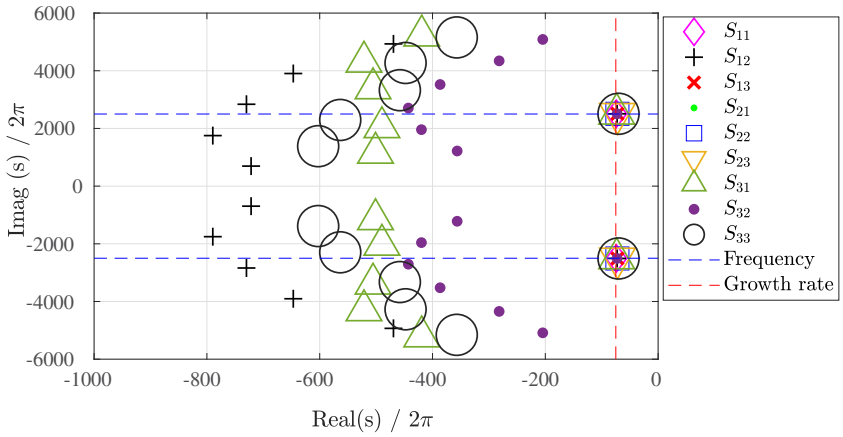

Fig. 8. Poles of each element of the scattering matrix plotted in the complex s plane. The dashed horizontal and vertical lines denote the frequency and growth rate of the ITA oscillations obtained from the Gaussian-Evolution computation.

Euler equation (LEE) framework. This section is organized as follows. An analytical expression governing the eigenvalues of the ITA feedback for an autoignition front is derived in Section 3.1. In Section 3.2, the sound field generated by an unsteady autoignition front in the one-dimensional setting is computed using the LEE framework and compared with the forced Euler computations. Section 3.3 discusses the results pertaining to the prediction of ITA modes associated with the autoignition front.

3.1. The dispersion relation for ITA modes associated with autoignition fronts

In simplified one-dimensional configurations, such as Fig. 2, it is common to compute the acoustic field by treating the reaction front as a spatial discontinuity which causes a jump in the mean flow quantities, and formulating a set of jump conditions linking the flow perturbations upstream and downstream of the front [10]. This approach is especially effective when the spatial extent of the flame is much smaller than the wavelength of the relevant acoustic modes under consideration. Both propagation and autoignition fronts harmonically change their position in response to acoustic disturbances. The importance of considering the flame motion when computing the combustor acoustic field was demonstrated by Chen et al. [19]. The effect of flame front motion is expected to also be important for autoignition fronts, since, in addition to acoustic velocity oscillations kinematically causing ignition front fluctuations, the pressure and temperature disturbances induced by an acoustic wave modulate the ignition chemistry causing oscillations in ignition time, which lead to oscillations in the flame position. A propagating flame is usually anchored by a mechanical flame holder or a recirculation zone, which impedes the flame movement under velocity fluctuations to some extent. Furthermore, due to the high sensitivity of the ignition time to temperature fluctuations and due to the direct effect of the ignition delay time on the front location, the movement of the flame can be expected to be much larger for autoignition fronts for a given acoustic perturbation magnitude.

The Rankine–Hugoniot jump conditions applied to a moving discontinuity [19,48] can be written in compact form in the frequency domain as

$$\mathbf{M}\begin{bmatrix} f_2 \\ g_1 \\ h_2 \end{bmatrix} = \mathbf{N}\begin{bmatrix} f_1 \\ g_2 \\ h_1 \end{bmatrix} + \mathbf{K}\widetilde{\dot{Q}} + \mathbf{J}\widetilde{X}_{\mathrm{ig}}, \tag{12}$$

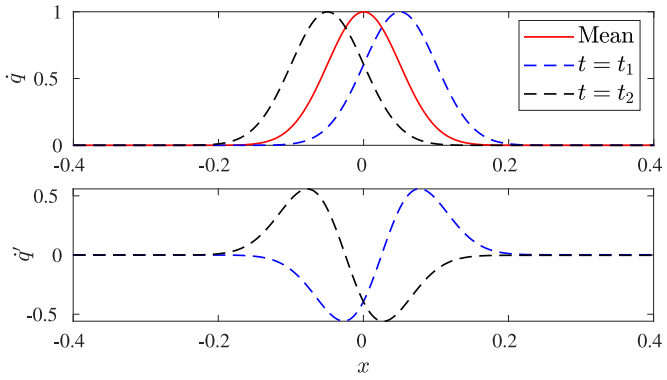

Fig. 9. Schematic illustrating the heat release rate fluctuations created due to ignition front motion. The top tile shows the instantaneous heat release rate profiles at two time instants in the ignition front oscillation cycle. The bottom tile depicts the fluctuations in the heat release rate created due to this ignition front motion.

where $\mathbf{M}, \mathbf{N}$ are 3x3 matrices, and $\mathbf{K}, \mathbf{J}$ are 3x1 vectors; their elements are given in the supplementary material. Eq. (12) can be rewritten by multiplying both sides by $\mathbf{M}^{-1}$ giving

$$\begin{bmatrix} f_2/p_0 \\ g_1/p_0 \\ h_2/p_0 \end{bmatrix} = \underbrace{\begin{bmatrix} T_2 & R_3 & T_3 \\ R_1 & T_1 & R_2 \\ T_4 & R_4 & T_5 \end{bmatrix}}_{\text{transmission and reflection}} \begin{bmatrix} f_1/p_0 \\ g_2/p_0 \\ h_1/p_0 \end{bmatrix} + \underbrace{\begin{bmatrix} S_3 \\ S_1 \\ S_5 \end{bmatrix} \frac{\widetilde{\dot{Q}}}{\dot{Q}_0} + \begin{bmatrix} S_4 \\ S_2 \\ S_6 \end{bmatrix} \frac{\widetilde{X}_{\mathrm{ig}}}{X_{\mathrm{ig0}}}}_{\text{generation by the ignition front}}, \tag{13}$$

where the R_i and T_i denote frequency-dependent functions that govern the reflection and transmission of the incoming characteristics to the outgoing characteristics by the ignition front. These terms are present even in the hypothetical case when the flame does not actively respond to the imposed disturbances ($\dot{Q}' = X'_{\mathrm{ig}} = 0$). The frequency response functions S_i govern the outgoing characteristics generated by the integrated heat release rate and ignition front position fluctuations, that is, the sound/entropy generated by an unsteady ignition front. While integrated heat release rate fluctuations ($\dot{Q}'$) act as a monopole source of sound [5], fluctuations in ignition front position (X'_{ig}) act as an (axially oriented) acoustic dipole. This is illustrated schematically in Fig. 9, where the fluctuating heat release rate profiles due to a pure ignition front motion ($\dot{Q}' = 0$) are plotted. The net effect of ignition length fluctuations is to create oscillations in the heat release rate, which ap-

pear as two distinct sources placed close to each other and oscillating with a phase difference of 180°, similar to an acoustic dipole [26].

Although the form of Eq. (13) has been derived keeping in mind the Rankine–Hugoniot jump conditions, it is, as such, more general and applies to ignition fronts with finite thickness. This is because Eq. (13), in essence, simply states that the outgoing characteristics are a linear combination of transmission and reflection of the incoming waves and the generation by the unsteady ignition front. Of course, care should be taken when applying Eq. (13) to combustor domains with complicated geometries. In such cases, additional terms due to, for example, acoustic reflection by solid walls can appear.

It is important to realize that Eq. (13) represents an open loop system: $\widetilde{\dot{Q}}$ and $\widetilde{X}_{ig}$ are treated as autonomous inputs, while in reality, they are dependent on the acoustic and entropy perturbations. Indeed, for autoignition fronts, $\widetilde{\dot{Q}}$ and $\widetilde{X}_{ig}$ intricately depend on how the various perturbations associated with an incident acoustic or entropy wave modify the ignition chemistry and the front kinematics and, therefore, depend on the flow perturbations in a non-trivial manner. Closed-loop dynamics of the ITA feedback can be obtained from Eq. (13) when the heat release rate and ignition front fluctuations associated with the autoignition front are related back to the acoustic and entropy perturbations via the flame transfer functions. For propagation-stabilized flames, it is common to write the integrated heat release rate fluctuations in terms of the velocity oscillations at some reference location upstream of the flame [49]. This makes sense because propagating flames stabilized at low Mach numbers mainly respond to velocity oscillations induced by an acoustic wave. For autoignition fronts, on the other hand, it is more appropriate to relate the flame response to the individual waves rather than to fluctuations in primitive variables. This is because prior works [17,18] have shown that acoustic and entropy waves modify the ignition chemistry differently and produce qualitatively different frequency responses in terms of the ignition length and global heat release rate fluctuations. Also, writing the heat release rate response in terms of velocity fluctuations does not take into account the influence of temperature disturbances induced by the entropy wave on the flame dynamics [17,50]. The flame response written in terms of the characteristic waves is, thus, written for the integrated heat release rate

$$\frac{\widetilde{\dot{Q}}}{\dot{Q}_0} = F_1(s)\frac{f_1}{p_0} + F_2(s)\frac{g_1}{p_0} + F_3(s)\frac{h_1}{p_0}, \tag{14}$$

and for the ignition length as

$$\frac{\widetilde{X}_{ig}}{X_{ig0}} = G_1(s)\frac{f_1}{p_0} + G_2(s)\frac{g_1}{p_0} + G_3(s)\frac{h_1}{p_0}. \tag{15}$$

In writing Eqs. (14) and (15), it is assumed that the autoignition front only responds to the fluctuations created by the characteristic waves upstream of the ignition front – f_1, g_1 and h_1. This is reasonable as it is these waves that modulate the autoignition chemistry and also introduce velocity oscillations upstream of the ignition front, creating fluctuations in the front position and the integrated heat release rate. In Eqs. (14) and (15), $F_i(s)$ and $G_i(s)$ represent the frequency-dependent flame transfer functions relating the heat release rate and ignition length fluctuations, respectively, to the characteristic waves. These transfer functions can be computed from three linearly independent forced Euler equation computations and are shown in the supplementary material. Figure 10 only plots the flame transfer functions relevant to the ITA feedback, i.e., F_2 and G_2. A system identification tool [47] is then used to identify a rational model, thus allowing to evaluate the transfer functions for complex values of ω (growing and decaying disturbances). The flame response transfer functions to an upstream-traveling acoustic

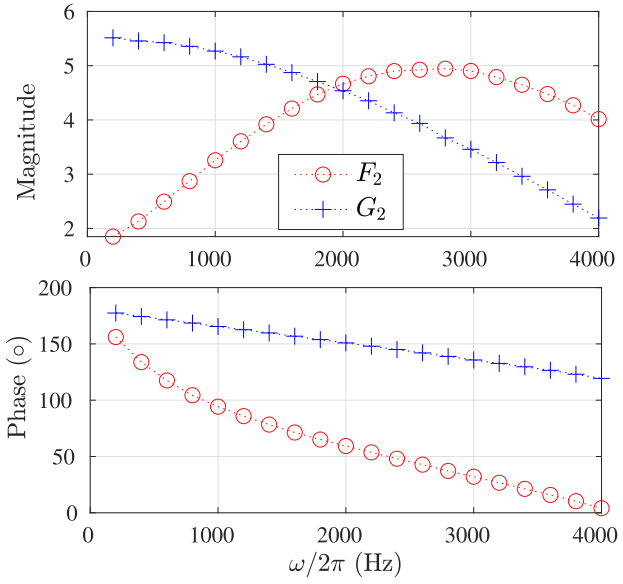

Fig. 10. Heat release rate and ignition length transfer function of the autoignition front to a g_1 wave.

(g_1) wave exhibit a distinct frequency-dependent character in gain and a time-delay-like behaviour in phase. A more detailed discussion on the frequency-dependent behavior of the transfer functions is given in prior works [17,18].

Eq. (13) is now modified to give insight into the dynamics of the ITA feedback by substituting Eqs. (14) and (15) for the flame response. The second row in Eq. (13), after this modification, reads

$$\frac{g_1}{p_0} = (R_1 + S_1F_1 + S_2G_1)\frac{f_1}{p_0} + (R_2 + S_1F_3 + S_2G_3)\frac{h_1}{p_0} + T_1\frac{g_2}{p_0} + (S_1F_2 + S_2G_2)\frac{g_1}{p_0}. \tag{16}$$

Eq. (16) reveals that the term g_1/p_0 is present in both the LHS (response) and the RHS (excitation) suggesting that a closed-loop feedback is established through the g_1 wave. Further simplification of Eq. (16) and comparison with the second row of the scattering matrix (10) yields

$$\frac{g_1}{p_0} = \underbrace{\left(\frac{R_1 + S_1F_1 + S_2G_1}{1 - S_1F_2 - S_2G_2}\right)}_{S_{21}}\frac{f_1}{p_0} + \underbrace{\left(\frac{T_1}{1 - S_1F_2 - S_2G_2}\right)}_{S_{22}}\frac{g_2}{p_0} + \underbrace{\left(\frac{R_2 + S_1F_3 + S_2G_3}{1 - S_1F_2 - S_2G_2}\right)}_{S_{23}}\frac{h_1}{p_0}. \tag{17}$$

The first and third rows of the Equation set (13) can also be expanded by substituting Eqs. (14), (15) and (17) into them. The steps involved in this procedure are omitted and we only present the final expression. The first row of Eq. (13) reads

$$\frac{f_2}{p_0} = \underbrace{\left((S_3F_1 + S_4G_1 + T_2) + (S_3F_2 + S_4G_2)S_{21}\right)}_{S_{11}}\frac{f_1}{p_0} + \underbrace{\left(R_3 + (S_3F_2 + S_4G_2)S_{22}\right)}_{S_{12}}\frac{g_2}{p_0} + \underbrace{\left((S_3F_3 + S_4G_3 + T_3) + (S_3F_2 + S_4G_2)S_{23}\right)}_{S_{13}}\frac{h_1}{p_0}. \tag{18}$$

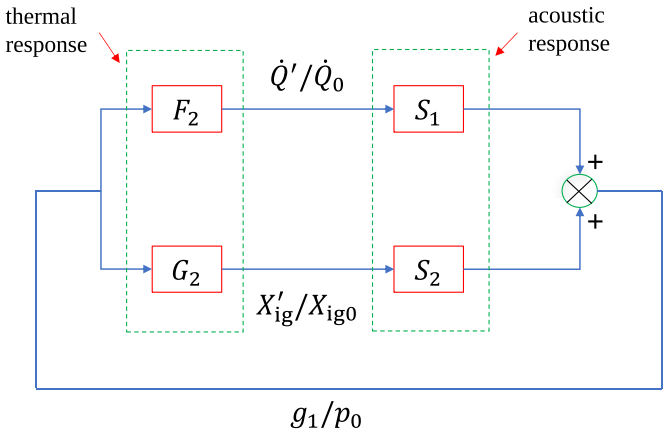

Fig. 11. Intrinsic thermoacoustic feedback loop in terms of the flame response and sound generation transfer functions.

The third row of Eq. (13) reads

$$\frac{h_2}{p_0} = \underbrace{\left((S_5F_1 + S_6G_1 + T_4) + (S_5F_2 + S_6G_2)S_{21}\right)}_{S_{31}} \frac{f_1}{p_0} + \underbrace{\left(R_4 + (S_5F_2 + S_6G_2)S_{22}\right)}_{S_{32}} \frac{g_2}{p_0} + \underbrace{\left((S_5F_3 + S_6G_3 + T_5) + (S_5F_2 + S_6G_2)S_{23}\right)}_{S_{33}} \frac{h_1}{p_0}. \tag{19}$$

Eqs. (18), (17) and (19) analytically express each row, and therefore each element, of the scattering matrix in terms of the frequency response functions governing the flame dynamics (F_i and G_i), the sound and entropy generation by the unsteady ignition front (S_i), and the reflection and transmission of acoustic and entropy waves by the ignition front (R_i and T_i). A crucial aspect to notice in Eqs. (18), (17) and (19) is that all the terms of the scattering matrix have a common denominator, given by the expression $D(s) = 1 - S_1F_2 - S_2G_2$. When $D(s)$ is close to zero, S_{21}, S_{22} and S_{23} reach high magnitudes resulting in significant amplification of the g_1 wave. Furthermore, we also observe from Eqs. (18) and (19) that both f_2 and h_2 are linear combinations of terms involving S_{21}, S_{22} and S_{23}. Therefore, when $D(s)$ is close to zero, significant amplification of f_2 and h_2 are also expected due to the large magnitudes of the elements S_{21}, S_{22} and S_{23}. This suggests that the frequency-dependent function $D(s) = 1 - S_1F_2 - S_2G_2$ can be factored out of the denominators of all the individual elements of the scattering matrix; consequently, the zeros of $D(s)$ govern the oscillation frequencies and growth rates of the intrinsic thermoacoustic modes. It can be noted that $D(s)$ only involves the frequency-dependent functions governing the thermal response of the ignition front to a g_1 wave (F_2 and G_2) and the generation of a g_1 wave by the unsteady ignition front (S_1 and S_2). This is to be expected as the ITA feedback mechanism, as depicted in Fig. 3, only involves the g_1 wave and the associated thermal and acoustic responses that it consequently produces. The ITA feedback loop is schematically shown in terms of the relevant flame response and sound generation transfer functions in Fig. 11.

To summarize, the prediction of the linear stability of the ITA oscillations associated with an autoignition front reduces to finding the complex valued quantity s satisfying

$$D(s) = 0, \quad \text{where} \quad D(s) = 1 - S_1F_2 - S_2G_2. \tag{20}$$

The real and imaginary parts of the solutions s correspond to the growth rate and angular frequency of the ignition front's ITA modes.

Next, we aim to predict the frequencies and growth rates of the ITA oscillations by solving Eq. (20), where F_2 and G_2 are taken from the forced Euler computations and S_1 and S_2 are determined from a suitable model for the combustor acoustics. Methodologies to compute the sound generation transfer functions using simplified approaches are discussed in Section 3.2.

3.2. Open-loop sound generation computation: Comparison between simplified models and forced Euler computations

In this section, two simplified approaches to compute the acoustic field associated with an unsteady autoignition front in the one-dimensional configuration are assessed by way of open-loop sound generation computations. Eq. (13) is solved in an open-loop fashion by specifying the incoming characteristic waves ($\widetilde{f_1}, g_2$ and h_1) and the thermal response of the autoignition front ($\widetilde{\dot{Q}}, \widetilde{X}_{ig}$) as inputs and thereafter computing the outgoing characteristic waves. We refer to these computations as 'open-loop' because the integrated heat release rate and ignition length fluctuations are treated as independent inputs, while in reality they are related to the acoustic and entropic disturbances [see Eqs. (14) and (15)]. The inputs for these computations, in order to be physically consistent and not arbitrary, are extracted from the forced Euler computations, and the resulting outgoing characteristics obtained from the simplified approaches are compared to the forced Euler data to assess their effectiveness. A minor technicality to be noted in this paper is that the term "sound generation" should not be understood in a literal sense as it includes both the generation of acoustic and entropy waves by the unsteady ignition front.

The two methodologies used in this work to compute the sound generated by an unsteady ignition front are (i) the analytical Rankine–Hugoniot jump conditions and (ii) a time-domain linearized Euler equation (LEE) solver. As explained previously, the Rankine–Hugoniot jump conditions applied to a moving ignition front take the form of a matrix Eq. (12), whose individual elements are listed in the supplementary material. As such, the Rankine–Hugoniot jump conditions represent an efficient way to describe the acoustic field associated with an unsteady autoignition front [32]. It only requires as inputs (see Eq. (12) and supplementary material) the integrated heat release rate fluctuations, ignition length fluctuations, the incoming characteristic wave amplitudes and the mean primitive variable values on either side of the ignition front. However, certain effects are not incorporated in this analytical framework; these are discussed in the following.

First, the detailed spatial structure of the mean and the fluctuating heat release rate are not taken into account since, in the analytical framework, the flame is treated as a discontinuous jump in the mean flow quantities. Second, autoignition fronts, by virtue of harmonic oscillations in their position, result in local fluctuations in gas properties, in addition to heat release rate oscillations, which contribute to additional sources of sound [23]. This situation is similar to that illustrated in Fig. 9 where, similar to the back and forth translation of the heat release rate profile associated with the ignition front, the gas property profiles also harmonically translate back and forth. This creates local fluctuations in gas properties, which show up as additional sources of sound in the linearized energy equation. Source terms involving gas property fluctuations cannot be trivially incorporated within the Rankine–Hugoniot analytical framework. To overcome these difficulties, we also describe the acoustic field associated with an unsteady autoignition front by a more detailed approach which involves a time domain-solution of the linearized Euler equations.

The linearized Euler equations are first derived by using the ansatz

$$\Phi(x,t) = \Phi_0(x) + \epsilon\Phi'(x,t), \tag{21}$$

for all primitive variables and gas properties (Φ) in the Euler Eq. (3). Grouping terms which are $O(\epsilon)$ gives the linearized Euler equations, which can be written in compact form as [23]

$$\frac{\partial \mathbf{U}'}{\partial t} + \mathbf{L}(\mathbf{U}_0)\mathbf{U}' = \mathbf{H}, \tag{22}$$

where $\mathbf{U}'$ is the vector of primitive variable fluctuations: $[\rho', u', p']^{\mathrm{T}}$. The linear operator $\mathbf{L}$, which acts on $\mathbf{U}'$, is composed of terms only involving the mean state $\mathbf{U}_0$ and the spatial derivatives. The time-dependent source terms are denoted by $\mathbf{H}$ and contain terms involving heat release rate ($\dot{q}'$) and gas property (γ', R') fluctuations, where γ is the specific heat ratio and R is the specific gas constant. The acoustic field generated by the unsteady ignition front is computed by specifying the source terms and marching Eq. (22) in time.

The ingredients essential to enable time-marching of the LEE are the mean primitive variable profiles, mean gas property profiles, boundary forcing and the time-dependent source terms. The source terms are essentially spatially resolved quantities describing the fluctuations of the heat release rate and the gas properties at each time instant. In this paper, these terms are first directly extracted from the forced Euler dataset at each time instant. We acknowledge that this approach of directly taking the source terms and the mean profiles from the forced Euler dataset is not the most elegant and relies heavily on the expensive Euler computations. However, the main point of this exercise is to assess the effectiveness of the analytical and the LEE approach in describing the combustor acoustic field. A more robust approach to specify the mean profiles and the time-dependent source terms will be provided subsequently in this section. Once the mean flow quantities and source terms are known, the linearized Euler equations are numerically solved in time using the dispersion relation preserving scheme [41]. The procedure to impose the characteristic based boundary conditions for the LEE, and the validation of the LEE framework with detailed DNS computations are given in previous work [23].

Figure 12 compares the magnitude and phase of the outgoing characteristic waves obtained from the two simplified approaches – Rankine–Hugoniot jump conditions and the LEE solver using source terms and mean profiles directly interpolated from the forced Euler computations (hereafter referred to as 'LEE-IS' computation) – with the forced Euler data. All the outgoing characteristic waves are normalized by the Fourier transform of the applied forcing which, for Fig. 12, corresponds to acoustic forcing at the inlet with an f_1 wave. Because of the intrinsic thermoacoustic feedback, significant amplification of the forcing is observed close to the frequency of the ITA mode (2500 Hz). It is also observed that both the Rankine–Hugoniot and the LEE framework capture the generation of the acoustic waves (g_1 and f_2) with good quantitative agreement. In terms of accuracy, the LEE approach is most effective, yielding identical amplitudes and phase of the outgoing acoustic waves in comparison to the forced Euler data. The Rankine–Hugoniot approach, on the other hand, shows a noticeable disagreement (around 15%) in the amplitudes of the acoustic waves in comparison to the forced Euler data at frequencies close to resonance.

The scenario is slightly different in the context of the entropy wave (h_2) computation from the simplified approaches in Fig. 12. While the LEE approach still demonstrates excellent agreement with the forced Euler data, the Rankine–Hugoniot approach, in comparison, yields large 'spurious' entropy wave amplitudes and incorrect phase. Previous work of Chen et al. [19] reported similar generation of spurious entropy waves in the context of one-dimensional propagation-stabilized flames. They observed that the generation of spurious entropy waves downstream of the flame arises due to neglect of the flame motion. While the amplitudes of the spurious entropy waves from the Rankine–Hugoniot approach are drastically reduced when flame motion is taken into consideration in Fig. 12 (see inset in $|h_2|/|f_1|$, which plots the entropy wave with neglected flame motion), however, we observe that they are not entirely eliminated even when the movement of the flame is taken into account. This warrants for an approach wherein a consistent, spatially fine-grained specification of the mean flow profiles and the fluctuating source terms are taken into account, similar to the LEE-IS approach, in order to eliminate the spurious entropy wave generation. This observation corroborates the recent findings of Meindl et al. [51] and Heilmann et al. [52] who proposed a linearized reactive flow solver and an arbitrary Lagrangian–Eulerian framework to take into account the fine-grained spatial resolution of the mean flow and the fluctuating source terms to suppress the generation of spurious entropy waves. The qualitative observations regarding the open-loop sound generation prediction using simplified approaches were similar for other forcing states (inlet entropic, exit acoustic) as well.

While the LEE-IS calculation computed the sound generation associated with an unsteady autoignition front with high accuracy, it is important to realize that it is not fully predictive in nature. This is because it relies on data from the unsteady forced Euler computation for the inputs, which includes the mean flow, gas property profiles and the spatio-temporal values of the heat release rate and gas property fluctuations. To overcome this difficulty, a method is proposed to construct the mean flow profiles and the time-dependent source terms using only the following inputs: the integrated heat release rate fluctuations, the ignition length fluctuations, the mean values of the primitive variables and gas properties on the unburnt and burnt side of the ignition front, and the mean ignition front position. This method is described next.

The spatial variation of the mean heat release rate can be constructed by assuming a Gaussian model for the heat release rate distribution [17] as

$$\dot{q}_0(x) = \frac{\dot{Q}_0}{\eta\sqrt{2\pi}} \exp\left(-\frac{(x - X_{\mathrm{ig}0})^2}{2\eta^2}\right), \tag{23}$$

where η represents the thickness parameter of the ignition front and $\dot{Q}_0$ is the mean integrated heat release rate given by

$$\dot{Q}_0 = \frac{\gamma}{\gamma - 1}(u_{02}p_{02} - u_{01}p_{01}) + \frac{1}{2}\left(\rho_{02}u_{02}^3 - \rho_{01}u_{01}^3\right), \tag{24}$$

where $()_{01}$ and $()_{02}$ denote mean quantities on the unburnt and burnt side, respectively. The instantaneous heat release rate at any time instant t is given by

$$\dot{q}(x,t) = \frac{\dot{Q}_0 + \epsilon\dot{Q}'}{\eta\sqrt{2\pi}} \exp\left(-\frac{(x - X_{\mathrm{ig}0} - \epsilon X'_{\mathrm{ig}})^2}{2\eta^2}\right), \tag{25}$$

where ϵ is a small parameter, and $\dot{Q}', X'_{\mathrm{ig}}$ are the integrated heat release rate and ignition length oscillations which are specified inputs. Eq. (25) is written by making use of the fact that the Gaussian profile translates axially due to ignition front fluctuations and changes in area due to integrated heat release rate oscillations. The linearized form of the fluctuating heat release rate can be obtained by subtracting Eq. (23) from Eq. (25), expanding the exponential term in a Taylor series, and then simplifying the resulting expression by only retaining terms which are $O(\epsilon)$ and neglecting all terms of higher order. This procedure yields the following expression for the fluctuating heat release rate:

$$\dot{q}'(x,t) = \exp\left(-\frac{(x - X_{\mathrm{ig}0})^2}{2\eta^2}\right)\left\{\frac{\dot{Q}'}{\eta\sqrt{2\pi}} + \frac{\dot{Q}_0}{\eta\sqrt{2\pi}}\frac{X'_{\mathrm{ig}}(x - X_{\mathrm{ig}0})}{\eta^2}\right\}. \tag{26}$$

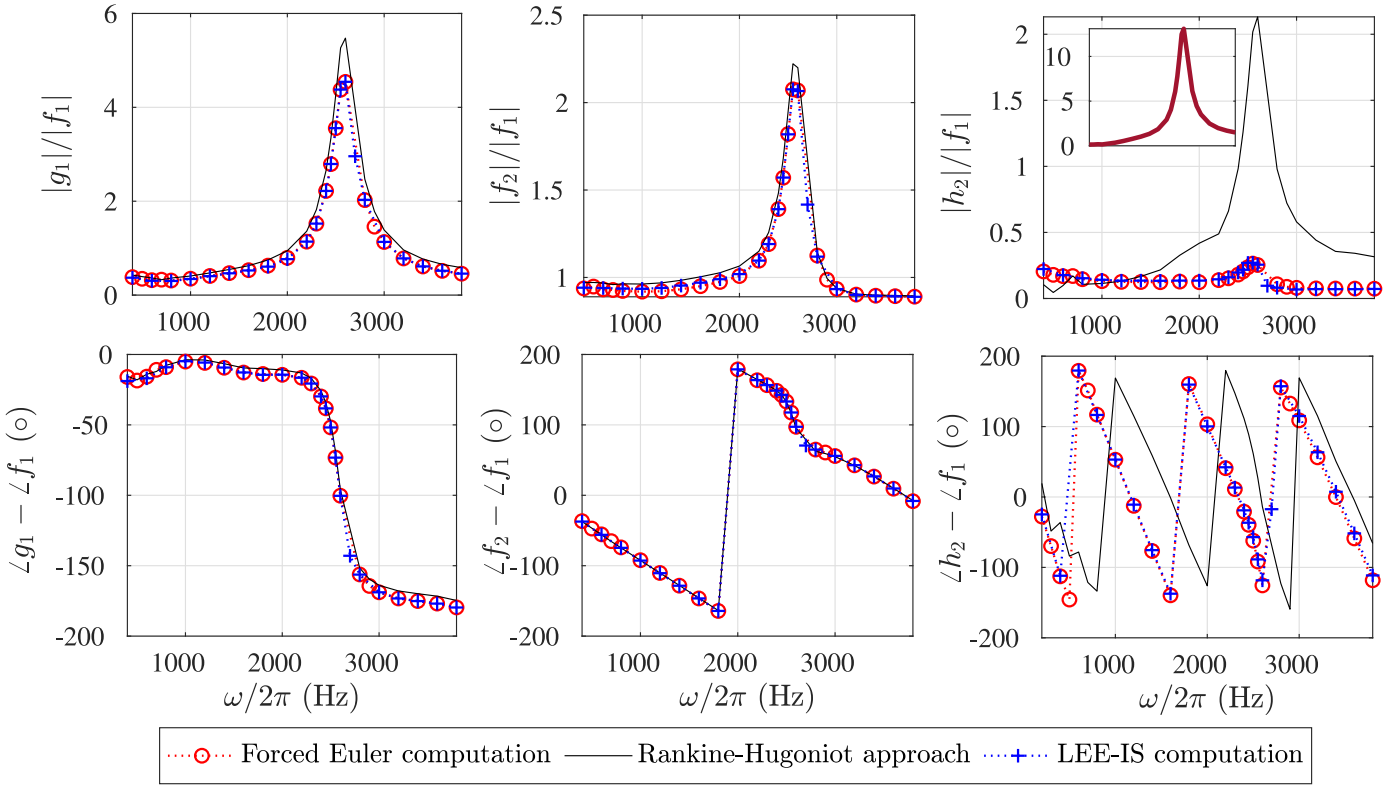

Fig. 12. Outgoing characteristic waves obtained from an open-loop computation using the Rankine–Hugoniot and LEE approaches and compared with the forced Euler computations. The ignition front is acoustically forced at the inlet via an f_1 wave. Inset in the $|h_2|/|f_1|$ plot shows the corresponding result from the Rankine–Hugoniot approach with neglected flame motion.

This can be visualized as two contributors to heat release rate fluctuations at any given point: (i) due to integrated heat release rate fluctuations and (ii) due to harmonic ignition front motion, which creates heat release rate fluctuations locally even in the absence of global heat release rate oscillations.

The spatial variation of the mean values of any primitive variable or gas property (Φ) can be constructed from the values of the corresponding quantities in the unburnt and burnt side and the ignition front thickness by using a smooth transitional model profile as

$$\Phi_0(x) = \Phi_{01} + \frac{1}{2}(\Phi_{02} - \Phi_{01})\left(1 + \mathrm{erf}\,\frac{x - X_{\mathrm{ig0}}}{\eta}\right). \tag{27}$$

To construct the fluctuating gas properties at any point at a time instant, the instantaneous value of any gas property (for example, the specific heat ratio γ) is written utilizing the form of Eq. (27) as

$$\gamma(x,t) = \gamma_{01} + \frac{1}{2}(\gamma_{02} - \gamma_{01})\left(1 + \mathrm{erf}\,\frac{x - X_{\mathrm{ig0}} - \epsilon X'_{\mathrm{ig}}}{\eta}\right). \tag{28}$$

In writing Eq. (28), it is implicitly assumed that the acoustic and entropy disturbances create negligible changes in gas properties and the main contributing factor to gas property fluctuations is the back and forth movement of the ignition front. The linearized fluctuations of the gas property γ can be obtained by subtracting Eq. (27) (for γ_0) from Eq. (28), writing the terms involving the error function in terms of its series expansions [53], and then only retaining the terms which are of order $O(\epsilon)$. The resulting fluctuations in gas property can be written as

$$\gamma'(x,t) = \frac{1}{\sqrt{\pi}}(\gamma_{02} - \gamma_{01})\left(-\frac{X'_{\mathrm{ig}}}{\eta}\right)\exp\left(-\frac{(x - X_{\mathrm{ig0}})^2}{\eta^2}\right). \tag{29}$$

Eqs. (23) and (27) for the spatial profiles of the mean heat release rate, primitive variable and gas properties, along with Eqs. (26) and (29) describing the fluctuations in heat release rate and gas properties, enable us to time march the LEE to determine the primitive variable fluctuations. Now, this procedure of constructing the source terms and mean profiles using model functions is, evidently, not physical because, the Gaussian profile for the mean heat release rate and the error function profile for the mean primitives/gas properties are not actual solutions of the time-averaged non-linear Navier–Stokes/Euler equations. Nevertheless, this approach of using model profiles, constructed using common mathematical functions, to represent mean flows has been used repeatedly in the past in the context of linear hydrodynamic instability analysis of canonical flows [54–56].

Figure 13 compares the spatial variations of the mean gas property and the mean heat release rate with the corresponding model profiles of Eqs. (27) and (23), respectively. While the model profiles capture the qualitative spatial variation of the mean quantities quite well, the match is not perfect, especially close to the mean ignition front location ($x = X_{\mathrm{ig0}} = 0.024$ m). However, coming up with better model profiles to fit the mean quantities more accurately is not the main objective of this work. Therefore, we simply use the Gaussian and error function profiles to construct the time-dependent source terms of Eq. (22) and, thereby, compute the sound generation from the unsteady autoignition front using the LEE solver. This open-loop LEE computation using constructed model profiles is hereafter referred to in this paper as 'LEE-CS' computation.

Figure 14 compares the magnitudes of the outgoing characteristic wave g_1 obtained from an open-loop LEE-CS computation with three other approaches: forced Euler data, LEE-IS computation and the Rankine–Hugoniot calculations. The forcing applied is identical to that in Fig. 12, which corresponds to velocity forcing at the inlet with an f_1 wave. From Fig. 14, it can be observed that the predictions of the g_1 wave with the LEE solver with source

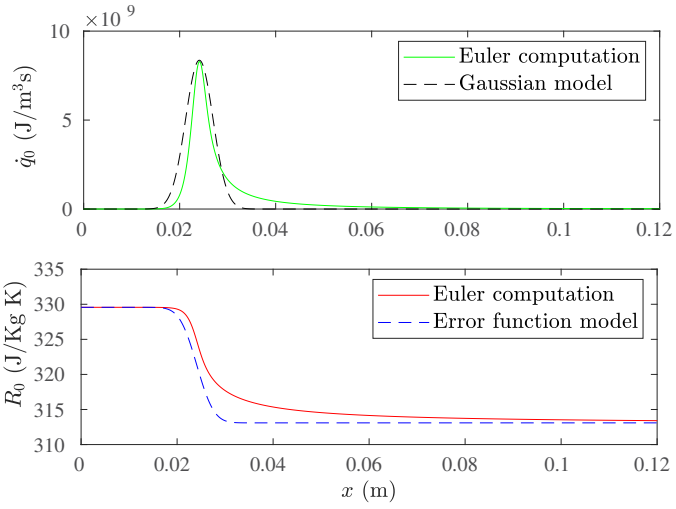

Fig. 13. Comparison between mean values of heat release rate (top) and gas property (bottom) with corresponding model profiles, where a value of 2.7 mm is used for the flame thickness parameter (η). The length of the reaction zone is around 25 mm which is approximately one-fourth of the h_2-wave's wavelength and one-seventh of the g_1-wave's wavelength at a frequency of 2500 Hz.

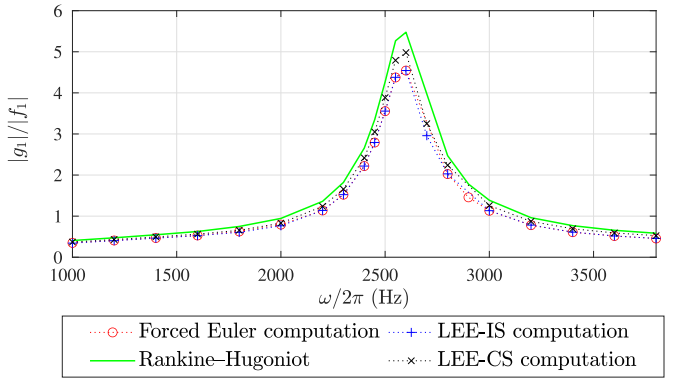

Fig. 14. Magnitudes of the outgoing characteristic wave g_1 obtained from the LEE-CS computation compared with other simplified and detailed approaches.

terms constructed from model profiles (LEE-CS) lies between the Rankine–Hugoniot predictions and the forced Euler results. On the one hand, the predictions of the g_1 wave from the LEE-CS computation deviate from the forced Euler results, especially close to resonance with deviations of around 9% in the magnitude. This deviation is mainly due to the behaviour seen in Fig. 13, where the model profiles fail to capture the precise spatial variations in the mean flow/gas property and the mean heat release rate close to the ignition front. The errors in these quantities then manifest as errors in the source terms of Eq. (22), which results in the deviations observed in Fig. 14. On the other hand, the LEE-CS computation brings down the errors associated with the Rankine–Hugoniot predictions noticeably. More specifically, inclusion of a finite (realistic) thickness to the ignition front and the inclusion of gas property fluctuations, both of which are not taken into account in a Rankine–Hugoniot framework, improves the prediction of the g_1 wave. The predictions of the other outgoing characteristics from the LEE-CS computation are plotted in the supplementary material.

To summarize, the results of this section demonstrate that the LEE framework, which numerically computes the fluctuations associated with a reacting flow characterized by a mean flow state and time-dependent source terms, proves to be most effective in predicting the acoustic field associated with an unsteady ignition front. Even when the mean flow quantities are approximated by model profiles constructed using standard functions, the LEE framework gives good estimates of the upstream traveling acoustic wave (g_1) generated by an unsteady ignition front. These results suggest that the LEE framework, in combination with flame transfer functions, can now be used to predict the eigenvalues characterizing the ITA oscillations associated with autoignition fronts, which is discussed in the next section.

3.3. Results: Prediction of frequency and growth rate associated with the ITA oscillations

In this section, the simplified approaches presented in Section 3.2 for computing the sound generated by an unsteady ignition front are employed to predict the frequencies and growth rates characterising the intrinsic thermoacoustic oscillations associated with these configurations. As already pointed out previously, the equation governing the thermoacoustic eigenvalues associated with the ITA feedback loop for an autoignition front is given by Eq. (20), which involves the flame response functions to a g_1 wave, F_2 and G_2, and the transfer functions governing the generation of a g_1 wave by the unsteady ignition front, S_1 and S_2. Here, we use the flame response functions extracted from the forced Euler computations in combination with the sound generation transfer functions obtained from the simplified approaches presented in Section 3.2 to solve Eq. (20).

Determination of S_1 and S_2 from the Rankine–Hugoniot approach is quite straightforward. Eq. (12) is considered first, all of whose terms only involve the mean flow parameters (see supplementary material). This equation is then transformed to the form of Eq. (13), yielding S_1 and S_2 directly in analytical form. To determine S_1 and S_2 from an LEE approach where the source terms and mean flow are constructed from model profiles (LEE-CS, see Section 3.2), two LEE computations are carried out. In the first computation, only the integrated heat release rate ($\dot{Q}'$) associated with the ignition front is perturbed in a harmonic fashion with small amplitude. The imposed forcing (f_1, h_1, g_2) and the ignition length perturbations (X'_{ig}) are all zero. This forcing scenario creates a heat release rate perturbation at each point in the domain through the first term of Eq. (26), which contributes to the source terms in Eq. (22), thereby generating acoustic and entropy perturbations. This calculation is repeated across a range of frequencies and the g_1 wave is measured at the inlet, enabling us to construct S_1. S_2 is similarly determined by performing a second LEE computation where only the ignition length (X'_{ig}) of the autoignition front is perturbed harmonically. Such a forcing scenario creates local heat release rate oscillations through the second term of Eq. (26), in addition to gas property fluctuations, which contribute to the sound generation.

Next, we discuss the determination of S_1 and S_2 from an LEE approach where the source terms and the mean flow are directly extracted from the forced Euler computations (LEE-IS, see Section 3.2). The source terms obtained from a forced Euler computation are due to the combined effect of integrated heat release rate and ignition length fluctuations. Thus, to separate out the individual contributions of these two effects, two linearly independent calculations need to be performed. First, the heat release rate and gas property fluctuations in the form of Fourier decomposed quantities at the forcing frequency are extracted from two linearly independent forced Euler computations. These two linearly independent forced Euler computations (say, I and II) can be composed of any two of the three linearly independent forcing states presented previously in Section 2.1. Second, the source terms, along with the mean flow, taken from the forced Euler computations are used as inputs to the LEE solver to compute the g_1 wave. The imposed acoustic/entropy forcing is set to zero for these two LEE computations, and only the fluctuating source terms (resulting from oscil-

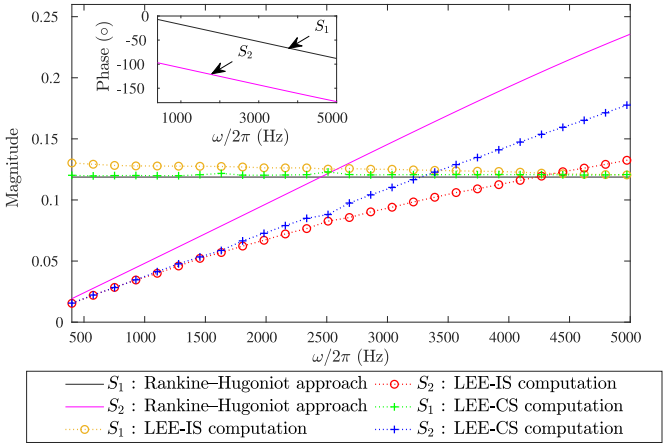

Fig. 15. Gain and phase (inset) of the sound-generation transfer functions S_1 and S_2, computed from various approaches.

lations of the ignition length, $\widetilde{X}_{\mathrm{ig}}$, and integrated heat release rate, $\widetilde{Q}$) act as sources of sound. Finally, the transfer functions S_1 and S_2 are determined from these two LEE computations by solving the following linear system

$$\begin{bmatrix} \left(\frac{\widetilde{Q}}{\bar{Q}_0}\right)^{\mathrm{I}} & \left(\frac{\widetilde{X}_{\mathrm{ig}}}{X_{\mathrm{ig}0}}\right)^{\mathrm{I}} \\ \left(\frac{\widetilde{Q}}{\bar{Q}_0}\right)^{\mathrm{II}} & \left(\frac{\widetilde{X}_{\mathrm{ig}}}{X_{\mathrm{ig}0}}\right)^{\mathrm{II}} \end{bmatrix} \begin{bmatrix} S_1 \\ S_2 \end{bmatrix} = \begin{bmatrix} (g_1/p_0)^{\mathrm{I}} \\ (g_1/p_0)^{\mathrm{II}} \end{bmatrix}, \tag{30}$$

where the superscripts I and II signify that the inputs for the two LEE calculations are taken from the two linearly independent forced Euler computations, I and II. In short, the second row of Eq. (13) is solved in an inverse manner to determine S_1 and S_2 with the imposed forcing set to zero and using the fluctuating source terms consistent with a forced Euler computation.

Figure 15 plots the gain and phase of the sound generation transfer functions (S_1 and S_2) relevant to the ITA feedback. The g_1 wave generated by integrated heat release rate oscillations, which is characterized by the transfer function S_1, exhibits an approximately constant gain across the frequency range considered. On the other hand, the g_1 wave generated by ignition length fluctuations, characterized by the transfer function S_2, shows an increasing gain with an increase in frequency. This frequency-dependent behaviour of the gain of the sound generation transfer functions S_1 and S_2 is qualitatively similar to the behaviour of an acoustic monopole and a dipole, respectively [57].

Figure 15 also compares the results obtained from the various simplified approaches used to compute the sound generation from unsteady ignition fronts. The transfer function phase is not shown for the various approaches since the differences were found to be negligible. The LEE-IS approach, due to its ability to compute the open-loop sound generation most accurately in comparison to the forced Euler (Section 3.2) and DNS computations [23], should be regarded as the benchmark against which other approaches are compared. Intuitively, it is easy to deduce that the differences, if any, between the three simplified approaches to compute the sound generation, should mainly show up in the transfer function S_2. This is because the primary difference between these approaches is in the level of detail with which the ignition front motion is described. The LEE-IS approach takes into account both the effects of local heat release rate and gas property fluctuations created due to ignition front motion. In addition, the LEE-IS approach also takes into account the exact spatial variations of the mean flow and the fluctuating source terms. On the other hand, the LEE-CS approach, while accounting for all the effects created due to ignition front motion, does not take into account the precise spatial distributions of the mean flow and fluctuating source terms. This effect, while relatively unimportant for the acoustic field generated by integrated heat release rate oscillations, is quite important to describe the acoustic field generated by ignition front oscillations. Indeed, as illustrated in Fig. 15, the transfer functions obtained from the LEE-CS computations mainly deviate from the results of the LEE-IS approach with regards to S_2, especially at higher frequencies.

The Rankine–Hugoniot approach does not take into account the detailed spatial variations of the mean flow profiles and the source terms either, as it treats the ignition front as a spatial discontinuity in the mean flow variables. Furthermore, the fluctuations in gas properties are not accounted for in this analytical framework. These effects show up as significant differences in the S_2 transfer function gain when compared to the LEE-IS and LEE-CS approaches in Fig. 15. The gain and phase of the transfer function S_1 show only very minor differences when computed using the different approaches.

Figure 16 plots $D(s)$, the frequency dependent function in Eq. (20), whose zeros govern the oscillation frequencies and growth rates of the ITA modes. Consistent with the observed oscillations, $D(s)$ goes close to zero near a frequency of 2500 Hz, which corresponds to the frequency of the ITA mode associated with the autoignition front. The LEE-IS approach and the LEE-CS approach exhibit similar frequency-dependent behaviour of $D(s)$, with slight differences in the phase close to the minimum of the gain curve.

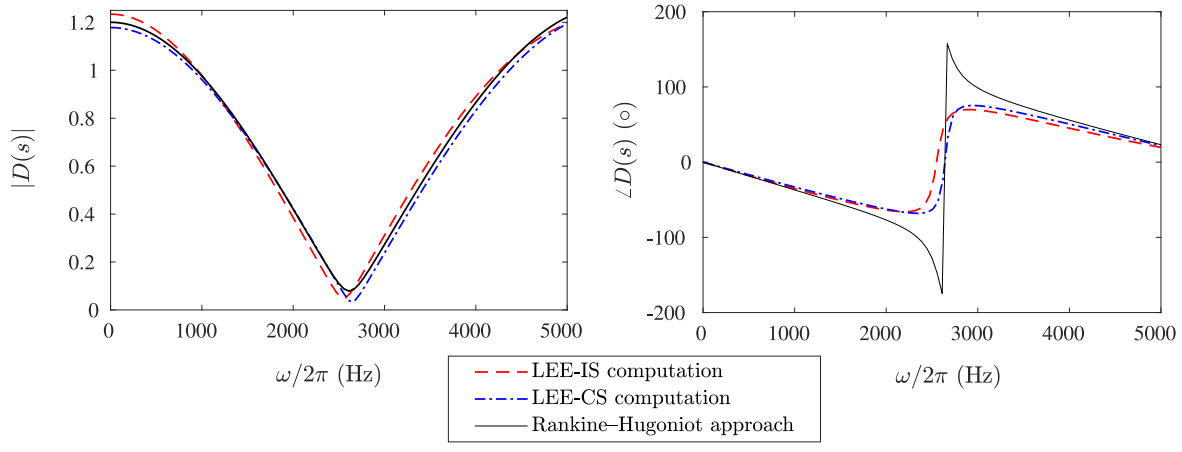

Fig. 16. (a) Magnitude and (b) phase of $D(s)$ as a function of frequency and at zero growth rate computed with various approaches.

Table 4
Complex eigenvalue s governing the dynamics of the ITA feedback, computed from various approaches. Note: only the most unstable eigenvalue is listed. Since $s = \mathrm{i}\omega$, a negative real part implies a stable mode and the imaginary part is the angular frequency of the oscillations.

Method to compute s/ω	$s/2\pi$, where $s = \mathrm{i}\omega$
Forced and unforced Euler computations	
Evolution of a Gaussian pulse (Fig. 4)	$-75 \pm 2500\mathrm{i}$
Band-pass filtering of forced response (Fig. 5)	$-74 \pm 2500\mathrm{i}$
Poles of the scattering matrix	See Table 3
Prediction: zeros of $D(s)$ with FTF from forced Euler computations	
LEE-IS approach	$-70 \pm 2551\mathrm{i}$
LEE-CS approach	$-49 \pm 2644\mathrm{i}$
Rankine–Hugoniot approach	$+115 \pm 2614\mathrm{i}$

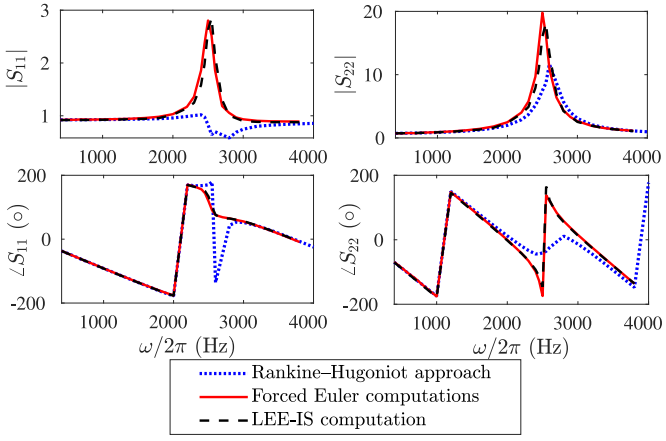

Fig. 17. Representative elements of the scattering matrix of the autoignition front computed from the Rankine–Hugoniot and LEE approaches and compared with the forced Euler computations.

The Rankine–Hugoniot approach, on the other hand, exhibits a noticeably different phase of $D(s)$ close to the frequency of the ITA mode of the system. In particular, the phase drops by π in contrast to an increase by π for the LEE approaches. This indicates opposite stability behaviour.

Table 4 lists the zeros of $D(s)$ obtained from the LEE and Rankine–Hugoniot approaches. The LEE-IS approach gives the best estimate of the frequency and growth rate of the intrinsic thermoacoustic oscillations, which lie within 8% of the corresponding values obtained from the Euler computations. The LEE-CS approach still gives a good estimate of the frequency, but predicts a slightly smaller damping rate. The Rankine–Hugoniot approach, on the other hand, gives a good estimate of the oscillation frequency, but predicts an unstable mode (positive growth rate), which is inconsistent with the ignition front behaviour observed in the Euler computations.

A graphical confirmation of the effectiveness of the LEE-IS approach in computing the thermoacoustic eigenvalues of the ITA feedback can be obtained by looking at the predictions of two representative elements of the scattering matrix in Fig. 17. The terms of the scattering matrix are computed using Eqs. (18), (17) and (19), where the transfer functions governing the transmission, reflection and generation of acoustic and entropy waves (T_i, R_i and S_i) by the unsteady ignition front are determined using the LEE solver. Also shown for comparison is the corresponding result from the Rankine–Hugoniot approach. The terms of the scattering matrix predicted using the LEE approach show an excellent match with the forced Euler computations, demonstrating the effectiveness of the LEE approach in predicting the ITA modes of the system. The predictions of all the other terms of the scattering matrix show a similar trend and are, therefore, omitted.

Lastly, we attempt to understand better why the Rankine–Hugoniot jump conditions incorrectly predicts the growth rate of the ITA modes of the autoignition front. As pointed out previously, the jump conditions make two main simplifying assumptions: zero thickness of the ignition front and constant gas properties. It is not clear which of these assumptions results in incorrect predictions of the ITA growth rates. To first understand the effect of assuming constant gas properties (and therefore neglecting the source terms due to gas property fluctuations), we repeat both the LEE-IS and LEE-CS calculations assuming constant gas properties. The S_2 transfer function gain from these computations is plotted in Fig. 19 and reveal interesting aspects, which are discussed next.

Firstly, assuming constant gas properties has a noticeable effect on the gain of the S_2 transfer function, even in the low frequency

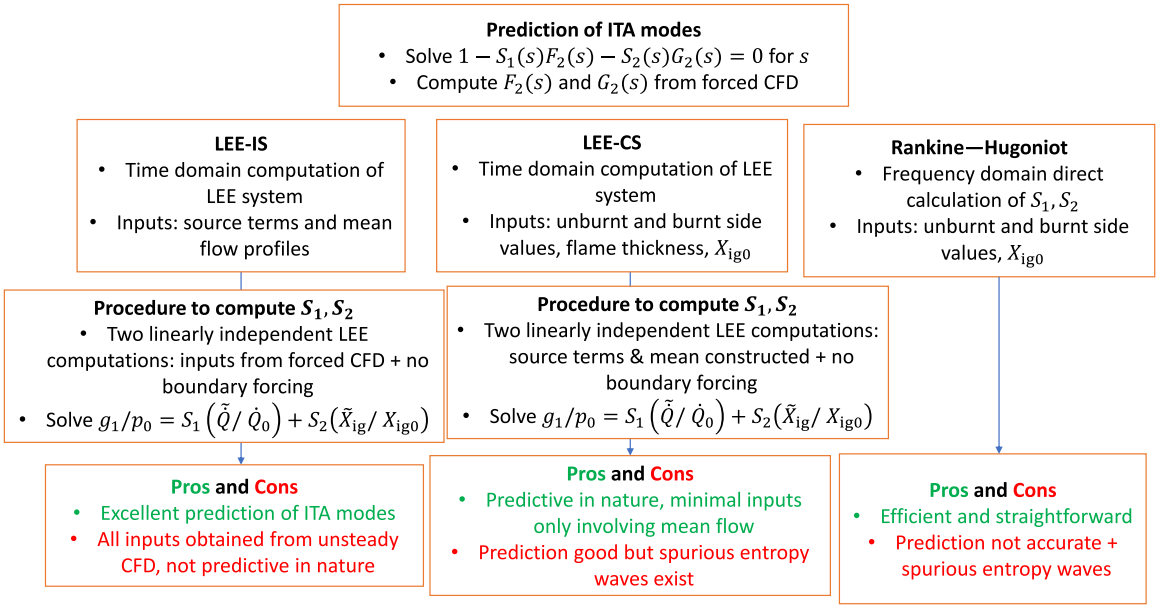

Fig. 18. Graphical chart describing the model structure and comparison of various models used to predict ITA modes of an autoignition front in this article.

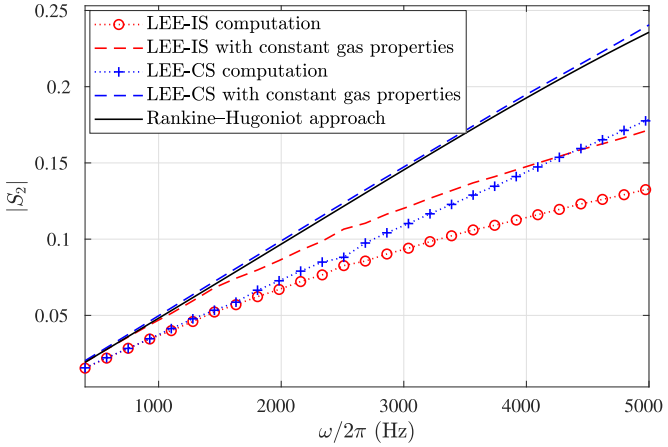

Fig. 19. Effect of assuming constant gas properties on the gain of the sound generation transfer function S_2.

region ($\omega/2\pi$ less than 2500 Hz). Discrepancies in the gain of S_2 in the low frequency range are expected to impact the ITA eigenmodes, since, in the expression for $D(s)$ [Eq. (20)], S_2 multiples G_2 and G_2 exhibits low-pass behaviour (see Fig. 10). Furthermore, the phase of the dispersion relation near the system eigenfrequency (2500 Hz) determines the growth rate associated with the eigenmode. Solving Eq. (20) using the sound generation transfer functions obtained from LEE-IS approach with constant gas properties resulted in the eigenvalues 78 ± 2503i for the ITA modes. This reveals that just assuming constant gas properties in the LEE-IS computation results in an unstable ITA growth rate prediction, which is even qualitatively incorrect to the observed dynamics. This significant variation in the ITA eigenvalues when assuming constant gas properties was observed for the LEE-CS approach as well.

Secondly, Fig. 19 suggests that the effects of neglecting the precise spatial variations of the mean flow profiles and time-dependent source terms mainly show up at higher frequencies. This can be seen by a comparison of the LEE-IS and LEE-CS approaches (both with constant and varying gas properties). This is not surprising since details of the spatial variation and impact of the thickness of the ignition front become important for short wavelengths of acoustic waves. Nevertheless, Fig. 19 and Table 4 reveal that not taking into account the precise spatial variations of the mean flow and source terms has noticeable effects on the S_2 transfer function gain at high frequencies, which results in minor deviations in the ITA growth rates.

The preceding discussion suggests that with regards to the Rankine–Hugoniot jump conditions, assuming constant gas properties is the main culprit in the incorrect prediction of ITA eigenvalues. While the zero thickness assumption also induces errors in the computation of S_2 transfer function, this effect is noticeable only at high frequencies and has a relatively minor effect on the phase of the dispersion relation close to the ITA eigenfrequency (and therefore, on the growth rates). An alternative route to the same conclusion is presented in the supplementary material.

To summarize, the comparison of predicted eigenvalues from various simplified approaches in Table 4 illustrates that the LEE framework is highly effective in predicting, with high accuracy, the stability of the ITA subsystem associated with an autoignition front in a reheat combustor. Furthermore, specifying the precise spatial variations of the mean flow and the fluctuating source terms to the LEE framework is essential to obtain accurate estimates of the ITA eigenvalues. The LEE framework, originally proposed in [23], can be a good starting ingredient for tools used to predict the thermoacoustic stability of complex laboratory and industrial-scale reheat burners. A pictorial representation of the stability framework employed in this article is presented in Fig. 18

4. Conclusions

Intrinsic thermoacoustic oscillations may generally occur when the flame response gain is large [6,7]. As previous work on the dynamics of autoignition-stabilized flames has shown, the response to temperature perturbations can be very large [50], in fact, an order of magnitude larger than what is frequently observed for propagation-stabilized flames. ITA oscillations are, hence, crucial to consider in systems with autoignition-stabilized flames.

In this paper, intrinsic thermoacoustic oscillations in a simplified one-dimensional reheat combustor with an autoignition-stabilized flame were investigated by means of computation and theory. In the context of autoignition fronts, intrinsic thermoacoustic feedback arises when an upstream-traveling acoustic wave, generated by heat release rate and ignition front perturbations, modulates the temperature, pressure and velocity of the incoming reactant mixture. These flow perturbations, introduced in the reactant mixture, modulate the autoignition chemistry, which, in turn, creates oscillations in the ignition front position and the heat release rate, thus closes the feedback loop. Reactive Euler equation computations of an autoignition front in a configuration with fully non-reflecting boundaries revealed the existence of an intrinsic thermoacoustic mode, which manifests as harmonic oscillations in the ignition front position and heat release rate at a distinct frequency. Analytically expressing the flame–acoustic interactions associated with an autoignition front in terms of the flame response and sound generation transfer functions revealed that the linear dynamics of the ITA mode is primarily governed by the transfer functions relating the response of an autoignition front to a g_1 (upstream-traveling acoustic) wave and the g_1 wave generated, in turn, by the unsteady flame response.

Using this insight, the linear stability characteristics of the ITA oscillations associated with the autoignition front were predicted using a hybrid methodology. In this hybrid approach, the thermal response of the flame, in terms of the flame transfer functions, is extracted from the forced Euler computations, and suitable simplified frameworks are used for describing the acoustic field of the combustor. Two simplified approaches were assessed for their effectiveness in predicting the linear intrinsic thermoacoustic stability of the system: (i) based on the Rankine–Hugoniot jump conditions, and (ii) a time-domain linearized Euler equation (LEE) solver. The LEE approach predicted the linear stability eigenvalue of the ITA feedback with much better quantitative accuracy in comparison to the Rankine–Hugoniot approach. This suggests that the LEE framework used in this paper can serve as a foundational building block, upon which more complex frameworks can be added to predict the thermoacoustic stability characteristics of reheat combustors. The present work, hence, represents a useful contribution both from the viewpoint of getting insight into intrinsic thermoacoustic oscillations associated with autoignition fronts, and from the viewpoint of developing robust tools to predict thermoacoustic oscillations in reheat combustion systems.

Declaration of Competing Interest

The authors declare that they have no known competing financial interests or personal relationships that could have appeared to influence the work reported in this paper.

Acknowledgments

This publication has been produced with support from the NCCS Centre, funded under the Norwegian research program, Centres for Environment-friendly Energy Research (FME). This project has received funding from the the Research Council of Norway

(Norges forskningsråd) under the Reheat2H2 project (project number 295203).

Supplementary material

Supplementary material associated with this article can be found, in the online version, at doi:10.1016/j.combustflame.2023.112844.

References

[1] M.R. Bothien, A. Ciani, J.P. Wood, G. Fruechtel, Toward decarbonized power generation with gas turbines by using sequential combustion for burning hydrogen, J. Eng. Gas Turbines Power 141 (12) (2019).
[2] A. Ciani, J.P. Wood, A. Wickström, G.J. Rørtveit, R. Steeneveldt, J. Pettersen, N. Wortmann, M.R. Bothien, Sequential combustion in Ansaldo Energia gas turbines: the technology enabler for CO2-free, highly efficient power production based on hydrogen, Turbo Expo: Power for Land, Sea, and Air, Vol. 84126, American Society of Mechanical Engineers, 2020. p. V04AT04A041
[3] O. Schulz, U. Doll, D. Ebi, J. Droujko, C. Bourquard, N. Noiray, Thermoacoustic instability in a sequential combustor: large eddy simulation and experiments, Proc. Combust. Inst. 37 (4) (2019) 5325–5332.
[4] T.C. Lieuwen, V. Yang, Combustion instabilities in gas turbine engines: operational experience, fundamental mechanisms, and modeling, Progress in Astronautics and Aeronautics, American Institute of Aeronautics and Astronautics, Vol 210, 2005. Reston, Virginia
[5] W.C. Strahle, On combustion generated noise, J. Fluid Mech. 49 (2) (1971) 399–414.
[6] M. Hoeijmakers, V. Kornilov, I.L. Arteaga, P. de Goey, H. Nijmeijer, Intrinsic instability of flame–acoustic coupling, Combust. Flame 161 (11) (2014) 2860–2867.
[7] T. Emmert, S. Bomberg, W. Polifke, Intrinsic thermoacoustic instability of premixed flames, Combust. Flame 162 (1) (2015) 75–85.
[8] S. Bomberg, T. Emmert, W. Polifke, Thermal versus acoustic response of velocity sensitive premixed flames, Proc. Combust. Inst. 35 (3) (2015) 3185–3192.
[9] C.F. Silva, Intrinsic thermoacoustic instabilities, Prog. Energy Combust. Sci. 95 (2023) 101065.
[10] A.P. Dowling, The calculation of thermoacoustic oscillations, J. Sound Vib. 180 (4) (1995) 557–581.
[11] T. Lieuwen, H. Torres, C. Johnson, B. Zinn, A mechanism of combustion instability in lean premixed gas turbine combustors, J. Eng. Gas Turbines Power 123 (1) (2001) 182–189.
[12] T. Komarek, W. Polifke, Impact of swirl fluctuations on the flame response of a perfectly premixed swirl burner, J. Eng. Gas Turbines Power 132 (6) (2010).
[13] E. Courtine, L. Selle, T. Poinsot, DNS of intrinsic thermoacoustic modes in laminar premixed flames, Combust. Flame 162 (11) (2015) 4331–4341.
[14] C.F. Silva, T. Emmert, S. Jaensch, W. Polifke, Numerical study on intrinsic thermoacoustic instability of a laminar premixed flame, Combust. Flame 162 (9) (2015) 3370–3378.
[15] N.K. Mukherjee, V. Shrira, Intrinsic flame instabilities in combustors: analytic description of a 1-D resonator model, Combust. Flame 185 (2017) 188–209.
[16] A. Orchini, C.F. Silva, G.A. Mensah, J.P. Moeck, Thermoacoustic modes of intrinsic and acoustic origin and their interplay with exceptional points, Combust. Flame 214 (2020) 251–262.
[17] F. Gant, A. Gruber, M.R. Bothien, Development and validation study of a 1D analytical model for the response of reheat flames to entropy waves, Combust. Flame 222 (2020) 305–316.
[18] H.S. Gopalakrishnan, A. Gruber, J. Moeck, Response of auto-ignition-stabilized flames to one-dimensional disturbances: intrinsic response, J. Eng. Gas Turbines Power 143 (12) (2021) 121011.
[19] L.S. Chen, S. Bomberg, W. Polifke, Propagation and generation of acoustic and entropy waves across a moving flame front, Combust. Flame 166 (2016) 170–180.
[20] A. Ni, W. Polifke, F. Joos, Ignition delay time modulation as a contribution to thermo-acoustic instability in sequential combustion, Turbo Expo: Power for Land, Sea, and Air, Vol. 78552, American Society of Mechanical Engineers, 2000. p. V002T02A023
[21] D.G. Goodwin, R.L. Speth, H.K. Moffat, B.W. Weber, Cantera: an object-oriented software toolkit for chemical kinetics, thermodynamics, and transport processes, 2018, (https://www.cantera.org) Version 2.4.0.
[22] A. Gruber, M.R. Bothien, A. Ciani, K. Aditya, J.H. Chen, F.A. Williams, Direct numerical simulation of hydrogen combustion at auto-ignitive conditions: ignition, stability and turbulent reaction-front velocity, Combust. Flame 229 (2021) 111385.
[23] H.S. Gopalakrishnan, A. Gruber, J. Moeck, Computation of intrinsic instability and sound generation from auto-ignition fronts, J. Eng. Gas Turbines Power 145 (4) (2023) 041008.
[24] T. Schuller, T. Poinsot, S. Candel, Dynamics and control of premixed combustion systems based on flame transfer and describing functions, J. Fluid Mech. 894 (2020).
[25] W. Polifke, Modeling and analysis of premixed flame dynamics by means of distributed time delays, Prog. Energy Combust. Sci. 79 (2020) 100845.
[26] A.D. Pierce, Acoustics: an introduction to its physical principles and applications, Springer Nature, Switzerland, 2019.
[27] F. Nicoud, L. Benoit, C. Sensiau, T. Poinsot, Acoustic modes in combustors with complex impedances and multidimensional active flames, AIAA J. 45 (2) (2007) 426–441.
[28] B. Schuermans, V. Bellucci, C.O. Paschereit, Thermoacoustic modeling and control of multi burner combustion systems, Turbo Expo: Power for Land, Sea, and Air, Vol. 36851 (2003), pp. 509–519.
[29] M.R. Bothien, J.P. Moeck, A. Lacarelle, C.O. Paschereit, Time domain modelling and stability analysis of complex thermoacoustic systems, Proc. Inst. Mech. Eng. Part A J. Power Energy 221 (5) (2007) 657–668.
[30] S.R. Stow, A.P. Dowling, A time-domain network model for nonlinear thermoacoustic oscillations, J. Eng. Gas Turbines Power 131 (3) (2009).
[31] M. Zellhuber, B. Schuermans, W. Polifke, Impact of acoustic pressure on autoignition and heat release, Combust. Theor. Model. 18 (1) (2014) 1–31.
[32] F. Gant, A. Cuquel, M.R. Bothien, Autoignition flame transfer matrix: analytical model versus large eddy simulations, Int. J. Spray Combust. Dyn. 14 (1–2) (2022) 72–81.
[33] A.S. Morgans, C.S. Goh, J.A. Dahan, The dissipation and shear dispersion of entropy waves in combustor thermoacoustics, J. Fluid Mech. 733 (2013).
[34] D. Wassmer, B. Schuermans, C. Paschereit, J. Moeck, Measurement and modeling of the generation and the transport of entropy waves in a model gas turbine combustor, Int. J. Spray Combust. Dyn. 9 (4) (2017) 299–309.
[35] T. Poinsot, D. Veynante, Theoretical and numerical combustion, RT Edwards, Inc., Philadelphia, PA, USA, 2005.
[36] T.J. Poinsot, S. Lele, Boundary conditions for direct simulations of compressible viscous flows, J. Comput. Phys. 101 (1) (1992) 104–129.
[37] J.C. Sutherland, C.A. Kennedy, Improved boundary conditions for viscous, reacting, compressible flows, J. Comput. Phys. 191 (2) (2003) 502–524.
[38] H.S. Gopalakrishnan, Dynamics and stability of autoignition fronts in elementary reheat combustor configurations, NTNU, 2022 Ph.D. thesis.
[39] W. Polifke, C. Wall, P. Moin, Partially reflecting and non-reflecting boundary conditions for simulation of compressible viscous flow, J. Comput. Phys. 213 (1) (2006) 437–449.
[40] G. Daviller, G. Oztarlik, T. Poinsot, A generalized non-reflecting inlet boundary condition for steady and forced compressible flows with injection of vortical and acoustic waves, Comput. Fluids 190 (2019) 503–513.
[41] C.K. Tam, J.C. Webb, et al., Dispersion-relation-preserving finite difference schemes for computational acoustics, J. Comput. Phys. 107 (2) (1993) 262–281.
[42] J. Li, Z. Zhao, A. Kazakov, F.L. Dryer, An updated comprehensive kinetic model of hydrogen combustion, Int. J. Chem. Kinet. 36 (10) (2004) 566–575.
[43] J.H. Chen, A. Choudhary, B. De Supinski, M. DeVries, E.R. Hawkes, S. Klasky, W.-K. Liao, K.-L. Ma, J. Mellor-Crummey, N. Podhorszki, et al., Terascale direct numerical simulations of turbulent combustion using S3D, Comput. Sci. Discov. 2 (1) (2009) 015001.
[44] C.L. Phillips, J.M. Parr, E.A. Riskin, T. Prabhakar, Signals, systems, and transforms, Prentice Hall, Upper Saddle River, NJ, USA, 2003.
[45] W.T. Thomson, Theory of vibration with applications, CRC Press, London, UK, 2018.
[46] R.J. LeVeque, et al., Finite volume methods for hyperbolic problems, Vol. 31, Cambridge University Press, Cambridge, UK, 2002.
[47] B. Gustavsen, A. Semlyen, Rational approximation of frequency domain responses by vector fitting, IEEE Trans. Power Deliv. 14 (3) (1999) 1052–1061.
[48] B.-T. Chu, On the generation of pressure waves at a plane flame front, Symposium (International) on Combustion, Vol. 4, Elsevier (1953), pp. 603–612.
[49] K. McManus, T. Poinsot, S.M. Candel, A review of active control of combustion instabilities, Prog. Energy Combust. Sci. 19 (1) (1993) 1–29.
[50] M. Bothien, D. Lauper, Y. Yang, A. Scarpato, Reconstruction and analysis of the acoustic transfer matrix of a reheat flame from large-eddy simulations, J. Eng. Gas Turbines Power 141 (2) (2019).
[51] M. Meindl, C.F. Silva, W. Polifke, On the spurious entropy generation encountered in hybrid linear thermoacoustic models, Combust. Flame 223 (2021) 525–540.
[52] G. Heilmann, T. Liu, P. Romero Vega, T. Sattelmayer, A novel decomposition approach preventing spurious entropy generation in hybrid thermoacoustic stability computations, J. Eng. Gas Turbines Power 144 (9) (2022) 091013.
[53] M. Abramowitz, I.A. Stegun, Handbook of mathematical functions with formulas, graphs, and mathematical tables, Vol. 55, US Government Printing Office, 1964.
[54] P.J. Schmid, D.S. Henningson, Stability and transition in shear flows, Vol. 142, Springer Verlag, New York, USA, 2001.
[55] K. Oberleithner, M. Sieber, C. Nayeri, C. Paschereit, C. Petz, H.-C. Hege, B. Noack, I. Wygnanski, Three-dimensional coherent structures in a swirling jet undergoing vortex breakdown: stability analysis and empirical mode construction, J. Fluid Mech. 679 (2011) 383–414.
[56] K. Manoharan, S. Hemchandra, Absolute/convective instability transition in a backward facing step combustor: fundamental mechanism and influence of density gradient, J. Eng. Gas Turbines Power 137 (2) (2015).
[57] P.M. Morse, K.U. Ingard, Theoretical acoustics, Princeton University Press, New Jersey, USA, 1986.